universität wien

MASTER'S THESIS

Title of the Master's Thesis

„Brain lesions in experimental neuromyelitis optica“

submitted by

Maria Magdalena Vogl, BSc

in partial fulfilment of the requirements of the degree of

Master of Science (MSc)

Vienna, 2016

Degree programme code as it appears on the student record sheet:	A 066 834
Degree programme as it appears on the student record sheet:	Masterstudium Molekulare Biologie
Supervisor:	Assoc. Prof. Dr. Monika Bradl

Acknowledgments

I kindly thank the team of the Neuroimmunology department for their warm welcome and fantastic working atmosphere. Most of all I want to express my gratitude to Assoc. Prof. Dr. Monika Bradl, who gave me the opportunity to work on different projects to expand my knowledge and refine my skills. I also thank Marianne Leiβer for her endless patience when explaining me immuno-histochemistry techniques. At last, I want to express my special thanks to Bleranda Zeka who always had an open ear for me and provided me with great advice.

I want to dedicate my master thesis to my family and friends who were with me and supported me through all the stressful times and celebrated with me my successes - without them I would have never come so far.

Content

1. Abstract

Neuromyelitis optica (NMO) is an inflammatory and astrocyte-destructive disease of the central nervous system which leads subsequently to demyelination. Most effects are seen in the optic nerves and in the spinal cord; abnormalities are less pronounced in the brain. Additionally, many NMO patients carry pathogenic serum autoantibodies, termed NMO immunoglobulins (IgGs), against the water channel aquaporin 4 (AQP4) which is especially enriched in the astrocytic end-feet. Typical NMO lesions contain activated microglia/macrophages, few T cells, a high number of neutrophils, deposition of complement and show a distinct loss of astrocytes.

This study focused on the characteristic pathological features in the brain of NMO animal models and the influence of T cell specificity on the distribution pattern of lesions with AQP4 loss. Therefore, archived brain material of Lewis rats was analysed. These animals had been injected with five different CNS specific T cell lines to provoke experimental autoimmune encephalomyelitis (EAE) and additionally with two different pathogenic NMO IgGs. All T cell lines had the ability to cross the blood brain barrier (BBB) but only three of them were sufficiently reactivated in the CNS to initiate NMO-like lesions with AQP4 loss. Even though the three T cell lines led to a different lesion topography, medulla and brainstem were in all animal the lesion "hotspots" which is correlating with human NMO. Only some minor differences were found either due to species characteristics or T cell specificities.

The key observation of the study is that the T cell specificity and their activation degree in the CNS influenced the formation of astrocyte-destructive lesions in the brain. Autoantibodies need the possibility to enter the brain and additionally an inflammatory environment in the area of the targeted antigen to initiate lesions. Further investigation is needed to find the targeted antigen of the T cells initiating inflammation in NMO patients and to understand the mechanism of autoimmunity in the CNS to establish an even more representative animal model of this disease.

2. Zusammenfassung

Neuromylitis optica (NMO) ist eine entzündliche und Astrozyten zerstörende Erkrankung des zentralen Nervensystems (ZNS), die letztlich zu Demyelinisierung führt. Vor allem die optischen Nerven und das Rückenmark sind betroffen, wohingegen Veränderungen im Gehirn weniger ausgeprägt sind. Zusätzlich werden in vielen NMO Patienten pathogene Autoantikörper, NMO IgGs genannt, detektiert, die sich gegen den Wasserkanal Aquaporin 4 (AQP4) richten welcher vor allem an astrozytären Zellfortsätzen zu finden ist. Typische NMO-Läsionen weisen aktivierte Mikroglia/Makrophagen, einige T-Zellen, eine erhöhte Zahl an Neutrophilen und die Fixierung von Komplement auf, sowie einen deutlichen Verlust von Astrozyten.

Diese Studie untersucht die pathologischen Merkmale im Gehirn von Tiermodellen für NMO und den Einfluss der Spezifität der T-Zellen auf die Verteilung von Läsionen mit AQP4-Verlust. Dafür wurde archiviertes Gehirnmaterial von Lewis Ratten analysiert. Diesen Tieren wurden pathogene NMO IgGs gespritzt als sie die ersten Anzeichen einer ZNS-spezifischen T-Zell-induzierten EAE aufwiesen. Alle T-Zelllinien konnten, die Blut-Hirn-Schranke zu überwinden, aber nur drei wurden im ZNS genug reaktiviert um NMO-typische Läsionen mit AQP4-Verlust zu initiieren. Obwohl diese zu unterschiedlichen Topografien führten, waren Medulla und Stammhirn in allen Tieren die „Hotspots“ für Läsionen, was mit menschlicher NMO korreliert. Nur geringfügige Unterschiede - bedingt durch entweder Spezieseigenschaften oder T Zell-Spezifitäten - wurden gefunden. Die zentrale Beobachtung der Studie ist, dass die Spezifität der T-Zellen und ihr Aktivierungsgrad im ZNS die Bildung von Läsionen mit zerstörten Astrozyten im Gehirn beeinflusst. Autoantiköper brauchen neben der Möglichkeit in das Gehirn einzudringen, auch ein entzündliches Milieu im Bereichen des Gehirns mit dem passenden Antigen für die Läsionsbildung. Fortführende Untersuchungen sind notwendig, um das Antigen der Entzündung auslösenden T-Zellen zu finden und um die Mechanismen der Autoimmunität im Gehirn zu verstehen, damit ein repräsentativeres Tiermodel etablieren werden kann.

3. Introduction

Neuromyelitis optica (NMO)

Neuromyelitis optica (NMO) is an inflammatory astrocyte-destructive and demyelinating disease of the central nervous system (CNS). Most effects are seen in the spinal cord (Fig. 1a) and in the optic nerves (Fig. 1b). NMO patients suffer from unilateral or bilateral optic neuritis and transverse myelitis, in most cases over 3 and more vertebral segments, which can lead to ocular pain as well as loss of vision, or to loss of sensory or respectively motoric function. Abnormalities in the brain of NMO patients are less pronounced, but lesions are predominantly found in hypothalamus and brain stem sometimes extending to the third and fourth ventricle (Fig. 1c) (Nakashima et al 2006, Pittock et al 2006a, Pittock et al 2006b, Poppe et al 2005). Symptoms such as hiccough, nausea and acute neurogenic respiratory failure are results of lesions in the brain stem (Misu et al 2005, Pittock et al 2004, Wingerchuk et al 1999, Wingerchuk & Weinshenker 2003).

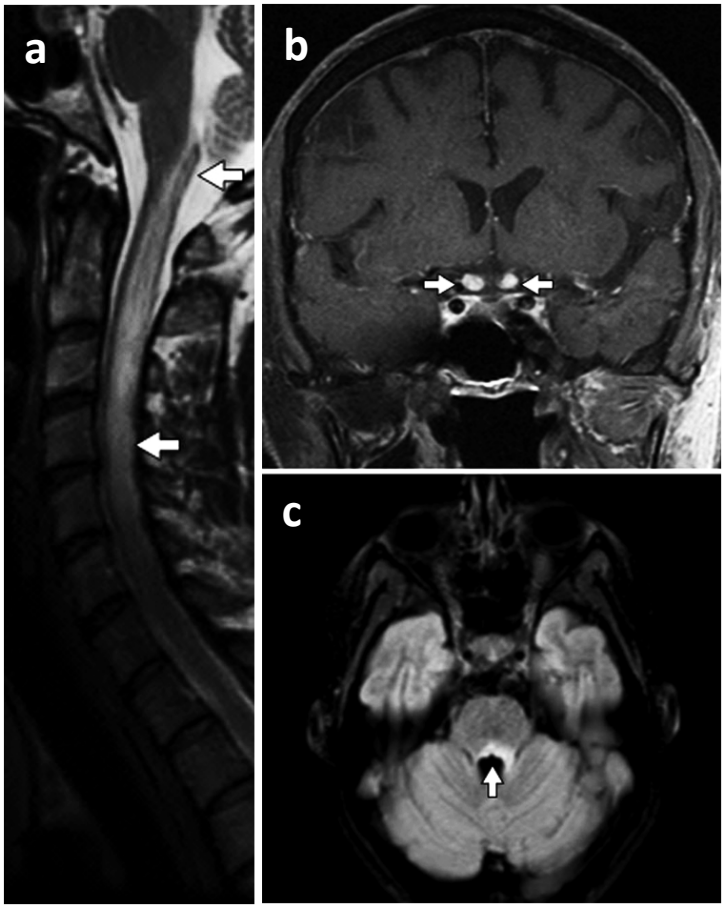

Fig. 1: Representative magnetic resonance images (MRIs) of NMO patients: Sagittal T2-weighted images of the cervical spine with a typical longitudinally extensive lesion over more than three vertebral segments and extending into the brainstem (a) with arrows indicating the borders of the lesion; bilateral optic nerve enhancement (b, arrows); signal abnormality next to the fourth ventricle in the region of the area postrema (c, arrow) (Flanagan & Weinshenker 2014)

In 1894, Devic and Gault were the first who reported the typical symptoms in humans and established the term neuromyelitis optica (Devic 1894; Gault 1894). Due to similarities like optic neuritis, myelitis and inflammatory demyelination NMO was thought to be a variation of MS (Cree et al 2002, de Seze 2003, de Seze et al 2003, Weinshenker 2003) for a long time. This changed over time and today there exist certain criteria for NMO, to distinguish it from other inflammatory demyelinating diseases shown in table 1 (Wingerchuk et al 2006).

One of three "additional criteria" is the presence of autoantibodies, termed NMO IgGs (Lennon et al 2004), against the water channel aquaporin 4 (AQP4) which is especially enriched in the astrocytic processes at the perivascular and subpial glia limitans (Lennon et al 2005). These antibodies are found in the vast majority of NMO

patients. NMO IgGs show pathogenicity, belong to the IgG1 subtype (Bradl et al 2009, Hinson et al 2007) and recognize epitopes within the extracellular loops of AQP4 (Nicchia et al 2009, Pisani et al 2011a).

However, not in all NMO patients who fulfill the diagnostic criteria summarized in table 1, NMO IgGs are found (Takahashi et al 2007, Waters & Vincent 2008). The missing NMO IgG titer might be the result of the low sensitivity in the applied assay or the fact that the patients carry an autoantibody against another unknown CNS antigen (Fujihara et al 2012). It could even point to mechanisms independent of the action of antibodies.

Table 1: Diagnostic criteria of NMO, table adapted (Wingerchuk et al 2006)

<table>
<tr><td colspan="3">NMO diagnostic criteria</td></tr>
<tr><td colspan="2">optic neurtitis</td><td>transverse myelitis</td></tr>
<tr><td colspan="3">Two of three additional criteria</td></tr>
<tr><td>longitudinally extensive spinal cord lesion extending over more than three vertebral segments</td><td>brain MRI abnormalities at onset not fulfilling the criteria for MS</td><td>NMO IgG seropositivity</td></tr>
</table>

The AQP4 protein is built-up of eight alpha helices which are connected by five loops, three of them are extracellular. Like all aquaporins it is organized in tetramers within the plasma membrane (Fu & Lu 2007, Gonen & Walz 2006, Verkman et al 2014) but AQP4 is the only one assembling in higher order structures called orthogonal arrays of particles (OAPs) (Rash et al 1998, Verbavatz et al 1997, Yang et al 1996). There exist two isoforms of human AQP4 one with the full length termed AQP4-M1 and one shorter isoform termed AQP4-M23 which is lacking 22 amino acids. The tetramers are in most times heterotetrameric (Neely et al 1999). The OAP formation only requires the M23 isoform whereby the amount of M1 in the assemblies influences the size of the OAPs, but the M1 isoform is not capable of forming homotetrameric OAPs

(Furman et al 2003, Rossi et al 2010, Yang et al 1996). In rats, the longer isoform AQP4 – Mz exists additionally (Rossi et al 2011) with a comparable function in the OAP formation as AQP4-M1 (Pisani et al 2011b) by restricting the assembly size but with a lower ability to bind NMO-IgGs (Rossi et al 2011).

To date it is not fully clear if NMO IgGs only target AQP4 in OAPs (Nicchia et al 2009, Pisani et al 2011a) or can also bind to AQP4-M1 tetramers although NMO IgGs often show a stronger binding to higher order assemblies of AQP4 (Iorio et al 2013, Mader et al 2010). There is a consensus that binding of OAPs results in a higher pathogenic potential due to different facts, such as binding of more than one NMO IgG molecule and the increased complement activation (Crane et al 2011, Hinson et al 2012, Phuan et al 2012).

AQP4 is the predominant water channel in the brain and the spinal cord (Papadopoulos & Verkman 2008) and allows passive transport of water in response to osmotic changes through the plasma membrane. It is enriched at the end-feet of astrocytes which play an important role in the BBB and the blood CSF barrier and can also be found on different other cell types as example retinal Müller cells, muscle cells and intestinal epithelium cells (Nielsen et al 1997, Rash et al 1998).

In consequence of the tight BBB NMO IgGs have only limited access to the CNS parenchyma and to enter the CNS from the periphery the autoantibodies need a more permeable BBB which exists naturally at some sites or can be a result of an injury or inflammation. After entering the CNS parenchyma, NMO IgGs can instantly bind AQP4 at the astrocytic end-feet of the glia limitans which leads to activation of complement and to subsequent attraction of inflammatory cells. These processes lead to astrocyte destruction and neuronal death causing the different neuronal symptoms and clinical features NMO patients experience (Wingerchuk et al 2007) and secondary demyelination ensues.

The characteristic histopathology of NMO patients reflects the previously described clinical features: inflammation in the spinal cord, the optic nerve and less prominent in the brain. Active lesions have an increased number of neutrophils and eosinophils as well as T cells and activated microglia/macrophages and show a typical rosette

pattern of Ig and complement fixation surrounding blood vessels (Lucchinetti et al 2002, Mandler et al 1993). A complete loss of AQP4 reactivity from the glia limitans up to the edge of the lesion can be observed (Misu et al 2007, Misu et al 2006, Roemer et al 2007, Sinclair et al 2007) and eventually also secondary demyelination and necrosis in grey and white matter.

Experimental autoimmune encephalomyelitis (EAE)

Although the knowledge about NMO, the autoantibody NMO IgG and its targeted antigen grew exponentially in the last years, developing a suitable animal model is still in progress, since injection of NMO autoantibodies into naïve animals didn't lead to experimental NMO (Bradl et al 2009). Currently, no long term, AQP4-specific antibody producing experimental NMO models exist, however it is possible to study important characteristics of human NMO in EAE/NMO models, such as the influence of the NMO IgGs, the impact of different CNS infiltrating cell types like CNS-specific T cells, and the cytokine involvement.

To induce NMO-like lesions, the NMO IgGs need to enter the CNS parenchyma to interact with their targeted antigen. In passive EAE Lewis rat models, pre-activated T cells-specific for different CNS antigens are used to render the BBB more permeable with the results enabling the serum proteins to enter the CNS parenchyma (Lassmann et al 1988, Linington et al 1988). The opening of the BBB coincides with the first symptoms of CNS inflammation like weight loss or loss of tail tonicity. Injection of NMO IgGs at this time point leads to similar pathological features as found in humans such as inflammatory infiltrates, binding of AQP4 leading to astrocyte-destructive lesions (Bennett et al 2009, Bradl et al 2009) and finally to demyelination (Bennett et al 2009). The CNS-specific T cells are reactivated in the CNS via MHC II+ complexes and their respective antigens on antigen presenting cells (APC) (Kivisakk et al 2009) leading to an inflammatory environment which is also an essential precondition to initiate NMO-like lesions in the model organisms.

The initial stages of NMO lesion formation are well represented in the EAE/NMO model but there are still some minor differences. The more complex astrocyte organisation and function in humans might lead to larger areas with damage than found in experimental rodent models. Furthermore, in contrast to a potential TH17 bias in humans, in the Lewis rats the disease is only TH1 cell-driven (Ishizu et al 2005). Also the polymorphonuclear cells differ, as humans have a higher amount of neutrophils in their blood than Lewis rats which has an impact on the size of lesions with AQP4 reactivity loss, whereby eosinophils are only found in NMO patients' lesions (Lucchinetti et al 2002) but not in EAE/NMO Lewis rats. However, the used rat strain might be in general unable to recruit eosinophils to the lesions in the CNS, regardless of the used CNS-specific T cells and antibody combination (Adelmann et al 1995, Storch et al 1998). NMO patients also show persistent vomiting (Apiwattanakul et al 2010, Popescu et al 2011) as a result of lesions in adjacent to or within the area postrema and the floor of the fourth ventricle (Popescu et al 2011). This symptom doesn't emerge in animal models even though lesions are sometimes found at the same sites (Yamamoto et al 2002).

Although not all NMO features are mirrored in animal models, correlating lesions are found in the optical nerves and the spinal cord (Zeka et al 2015), the most affected areas in NMO patients. The question arose if the animal models also represent in the same way the abnormalities found in the brain of NMO patients and which influence the EAE inducing T cell specificity has on the lesion topography?

Since the targeted antigen, of the lesion initiating T cells in NMO patients, is still unclear different surrogate T cells are needed to induce EAE. To investigate the lesion localisation in the brain of NMO animal models archived brain material of animals injected with pathogenic NMO IgGs at the onset of CNS-specific T cell-induced EAE were analysed.

4. Material and methods

The study was performed on archival brain tissue sections which derived from the below-mentioned papers (Bradl et al 2009, Pohl et al 2011, Pohl et al 2013, Zeka et al 2015). For these papers the following material and methods were used.

4.1 Animals

Lewis rats (7-8 weeks) were obtained from Charles River Wiga (Sulzfeld, Germany) and housed in the Decentral Facilites of the Institute for Biomedical Research (Medical University Vienna) under standardized conditions. The experiments were approved by the Ethic Committee of the Medical University Vienna, with the license of the Austrian Ministry for Science and Research. (Bradl et al 2009, Pohl et al 2011, Pohl et al 2013, Zeka et al 2015)

4.2 Preparation of NMO IgG

For the experiments, the preparation and purification of plasmapherisates of two different NMO IgG seropositive patients was essentially done as described (Coligan 1991). To preserve the patient's anonymity, the two plasmapheresis fractions will be subsequently referred to as NMO IgG J0 and NMO IgG 9. The method which was used to detect and titrate the human anti-AQP4 antibodies was previously described (Takahashi et al 2006, Takahashi et al 2007). The use of the patient-derived NMO IgG was approved by Ethics Committee of Tohoku University School of Medicine (No. 2007-327). As negative control, normal human IgG preparation was used (SubcuviaTM, Baxter, Vienna). (Bradl et al 2009, Pohl et al 2011, Pohl et al 2013, Zeka et al 2015)

4.3 Antigens

The following peptides and antigens were used for immunization and T cell isolation/ propagation:

Table 2: AQP4 peptides

Peptide	Amino acid sequence	MHC II epitopes
$AQP4_{207-232}$	YTGASMNPARSFG**PAVIM**GNWENHWI	p220–228: PAVIMGNWE
$AQP4_{268–285}$	**KAA**QQTKGSYMEVEDNRS	p271–279: QQTKGSYME
		p273–281: TKGSYMEVE

AQP4 peptides were synthesized by Centic Biotec (Germany) (Pohl et al 2011, Zeka et al 2015). Additionally, myelin basic protein (MBP, Sigma; (Bradl et al 2009)) from guinea pig, myelin oligodendrocyte glycoprotein (MOG, recombinant N-terminal peptide 1-125, rat own production; (Pohl et al 2013)) and astrocytic Ca2+ binding protein S100β (bovine, Sigma; (Pohl et al 2013)) were used.

4.4 T cell line preparation

Each animal was injected with 200 µl of a 1:1 mixture of the relevant antigen (stock 2 mg/ ml) in Freund's incomplete adjuvants supplemented with 4 mg/ ml mycobacterium tuberculosis H37Ta. The animals were sacrificed with CO_2 9-11 days after immunization; they were all clinically healthy and didn't show any signs of inflammation of the CNS or of peripheral organs. The lymph nodes closest to the immunization site were extracted and used to establish-specific T cell lines for two different AQP4 peptides ($AQP4_{207-232}$ (Pohl et al 2011), $AQP4_{268–285}$ (Zeka et al 2015)), myelin basic protein (MBP, (Bradl et al 2009)), myelin oligodendrocyte glycoprotein (MOG, (Pohl et al 2013)) and S100β (Pohl et al 2013) as previously described in (Ben-Nun et al 1981).

4.5 Experimental autoimmune neuromyelitis optica (ENMO) induction and tissue preparation

Induction of experimental autoimmune neuromyelitis optica (ENMO) was done by injecting in vitro activated T cell lines (number of injected T cells shown in Table 2 below) into the abdominal cavity of Lewis rats on day 0.

The weight loss of the animals was evaluated daily and the animals were examined for clinical signs of ENMO, i.e. for partial loss of tail tonus or for weakness of the hind limb. At day 4-5 after T cell injection, the animals showed the first signs of ENMO and received an intraperitoneal injection with 1 ml phosphate buffered saline (PBS) containing either 10 mg NMO IgG9/ NMO IgGJ0 or 10 mg normal human IgG (SubcuviaTM, Baxter, Vienna) or no further additives. Also some animals without T cell treatment were injected with the same amount of PBS containing NMO IgG J0 and PBS containing normal human IgG. After 24 hours (h) or 48 hours , the animals were sacrificed by an overdose of CO2 and perfused with 4% phosphate-buffered paraformaldehyde (PFA), then the brain was extracted and further fixed with 4% PFA for 18h. The fixed brain material was dissected and routinely embedded in paraffin. (Bradl et al 2009, Pohl et al 2011, Pohl et al 2013, Zeka et al 2015)

Table 3: numbers of injected T cells per animal

specify	MBP	$AQP4_{207-232}$	S100β	MOG	$AQP4_{268-285}$
injected T cells	1×10^6	$3.5\text{-}7 \times 10^7$	8×10^6	2×10^7	3×10^6; 2×10^7

4.6 Immunohistochemistry

The brains were cut into 2-4 µm thick sections on a microtome and stained using different antibodies and visualization methods (Aboul-Enein et al 2004). All incubation steps were made in a wet chamber to prevent dehydration during procedure.

4.6.1 Deparaffination and blocking peroxidase

The sections of the brains were dewaxed twice in xylene for 15 min and washed twice to 96% ethanol. To block the endogenous peroxidase the sections were incubated in 100% methanol with 0.2% H_2O_2 at room temperature for 30 min. After that, they were transferred to a series of descending concentrations of ethanol (96% to 70% to 50%) and then washed two times in distilled water.

4.6.2 Antibodies

The information about the used antibodies, their dilutions and pre-treatments are provided in tables 4 and 5.

Table 4: Antibodies information for rat brain sections

Primary AB	Target	Reactivity/ Clonality	Company	Pre-treatment	Secondary AB	possible extra
anti-- AQP4 (1:250)	astrocytes	rabbit polyclonal	Sigma, Germany	*x*	Bi α Rabbit (1:2000)	DAB x Co
ED1 (1:9000-10.000)	macrophages, microglia	mouse monoclonal	Serotec, Germany	***E** or **C***	Bi α mouse (1:200-1500)	
CD3 (1:2000)	T cells	rabbit polyclonal	NeoMarkers, Fremont, USA	***E** or **C***	Bi α Rabbit (1:600-2000)	CSA 1:1000 20min

Co = enhancement of DAB visualization with copper; *E* = EDTA buffer; *C* = citrate buffer

4.6.3 Pre-treatment

For pre-treatment, the sections were placed in a plastic coplin jar with citrate buffer (0.01M pH 6; ***C***) or EDTA-buffer (pH 8.5; ***E***), then incubated for 1h in a steamer (~100°C) and afterwards cooled to room temperature for 20min.

4.6.4 Blocking of unspecific background reactions

Fetal calf serum (FCS, 1:10; Life Tech, Austria) with DAKO buffer (Dako, Austria) was used for the background blocking for 15-20 min at room temperature and for the dilution of the different antibodies.

4.6.5 Primary and secondary antibodies

In between the application of the primary and secondary antibody and before the application of 3,3' diaminobenzidine-tetrahydrochloride (DAB) the sections were washed five times with tris-buffered saline (TBS). After blocking with FCS in Dako buffer, the primary antibodies were incubated at 4°C overnight and the secondary antibodies (GE Healthcare/Amersham) at room temperature for 1h. Then Avidin-peroxidase (Sigma; 1 mg dissolved in 1 ml distilled water) was applied for 1h at room temperature.

4.6.6 Catalysed Signal Amplification (CSA)

Method was used as essentially described previously (King et al 1997) with some modification from Jan Bauer (Wien) und Christian Bien (Bonn). Briefly, after the Avidin-peroxidase treatment of 1h at room temperature, the sections were treated with 50 µl CSA solution in 50 ml PBS and 50 µl H_2O_2 (30%) for 20 min at room temperature. Then they were washed with PBS and incubated again with Avidin-peroxidase for 30 min at room temperature.

4.6.7 Visualization with DAB and counterstaining with hematoxylin

As the final step, the Avidin peroxidase was visualized with DAB solution (Sigma, Germany) and counterstaining was done with hematoxylin. For the visualization, 1 ml DAB solution was diluted in 50 ml PBS and filtered before 16.5 µl H_2O_2 were

added and the sections were incubated with the solution for 5-10 min. For the counterstaining, the sections were treated with hematoxylin for 7-20 sec (depending on the required intensity), rinsed with tap water untill it stayed clear, plunged two times in HCl alcahol and incubated 5min in Scott´s solution. Then they went through a series of ethanol (from 50% to 96%) and ester (n-Butylacetat; Sigma) before they were embedded in Eukitt (O. Kindler, Germany) and dried overnight at 4°C.

4.7 Buffers and Solutions

PFA 4% 1L:

40 g of paraformaldehyde was dissolved in 500 ml warm Sörensen-buffer (0.2 M, pH 7.4) and 500 ml distilled water.

FCS/DP:

Fetal calf serum (Life Tech, Austria) diluted to 10% in DAKO buffer (DB) (DB stock solution from Dako, Austria was 1:10 diluted with distilled water for usage).

TBS 1L:

Tris-buffered saline (TBS) stock solution was prepared by dissolving 180 g NaCl, 60.57 g Tris in 400 ml 1 N HCl with 600 ml distilled water and adjusted pH to 7.5 with HCl. For the staining the stock solution was diluted 1:20 with distilled water and stored at room temperature.

PBS 2,5L:

The stock solution of phosphate-buffered saline (PBS) contained 13.8 g NaH_2PO_4 (0,04 M), 71.2 g Na_2HPO_4 (0,16 M) and 90 g NaCl and was filled up to 2.5 L with distilled water. For the working solution stock was diluted 1:4 with distilled water.

Citratbuffer 1L:

2.10 g citric acid was dissolved in 1 L distilled water.

EDTA-buffer 50 ml:

For the stock solution 1.21 g TRIS (10 mM) and 0.37 g EDTA (1 mM) were dissolved in 50 ml bi-distilled water and adjusted to pH 8.5. Then 2.5 ml of the stock were diluted with 50 ml bi-distilled water for usage.

CSA solution:

For the borate buffer 0.1545 g boric acid were dissolved in 50 ml distilled water and the pH was adjusted on 8 with NaOH. Next 15 mg sulpho NHS LCS Biotin (Pierce, P.O.B., USA) were added to 6 ml buffer then 4.5 mg tyramine and stirred overnight at room temperature. The solution was filtered and stored at -20°C in 50 µl aliquots.

DAB solution:

1 g DAB (dehydrate) was dissolved in 40 ml PBS then filtered and stored at -20 °C in 1 ml aliquots.

Scott solution:

Scott solution contained 2 g $KHCO_3$ and 20 g $MgSO_4$ x $7H_2O$ dissolved in 1 L distilled water.

HCl alcohol:

100 ml 70% alcohol with 0.5 ml concentrated HCl (37%)

Enhancement of DAB with copper:

10 g $CuSO_4$ (2%) and 4,5 g NaCl (0.9%) were dissolved in 500 ml distilled water and the slides were treated for max 5min.

4.8 Imaging

The analysis of the differently stained brain areas of interest was done using a Nikon H550S (Nikon, Austria) light microscope and were projected on brain schemes. For the imaging of the brain sections a Nano-Zoomer 2.0-HT Digital slide scanner from Hamamatsu was used and Photoshop CS4 for further editing.

5. Results

This study focused on the characteristic pathological features in the brain of NMO animal models and their differences depending on the T cell line used to induce EAE and the two different pathogenic antibodies NMO IgG J0 and NMO IgG 9.

To analyse the archived brain material via immunohistochemistry with two different stainings, clear defined characteristics had to be determined for an inflammatory lesion to qualify as NMO-like lesion. There must be: a complete loss of AQP4 reactivity from the glia limitans up to the edge of the lesion (Fig. 2a), together with infiltration of T cells (Fig. 2c) and activated microglia/macrophages (Fig. 2d). Areas with a more patchy loss of AQP4 (Fig. 2b), which showed still some AQP4 reactivity in particular at the glia limitans (Fig. 2b, arrows) were not considered as NMO-like lesions.

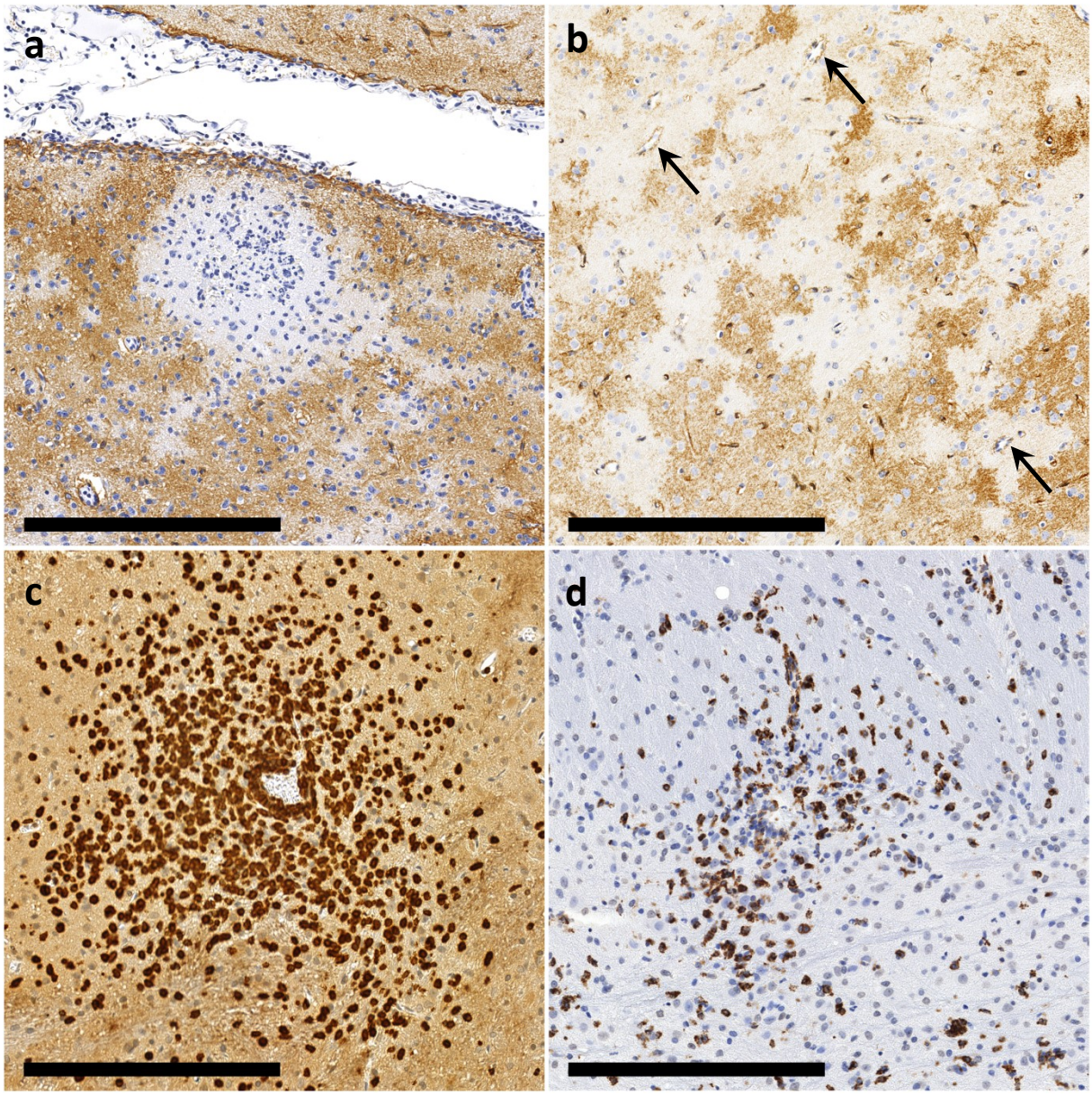

Fig. 2: Representative examples of NMO-like brain lesions (a, c, d) and additionally an area with a more patchy loss of AQP4 (b) and still some AQP4 reactivity left at the glia limitans (b, arrows), which were not considered as NMO-like lesions. Sections that were stained with anti-AQP4 antibody show the presence (brown) and the loss (white) of this protein (a, b), anti-CD3 antibody to show T cells (brown, c) and anti-ED1 antibody to reveal activated microglia and macrophages (brown, d). Counterstaining was done for all with hematoxylin to reveal nuclei (blue). Scale bars = 250 µm

5.1 T cell infiltration and location of lesions with AQP4 loss in the brain

In initial experiments, T cells inducing CNS inflammation and NMO IgG recognized different antigens. Is the location of lesions with AQP4 loss determined by the CNS antigen-specific T cells, or are there "hotspots" in the CNS which are especially vulnerable for the formation of lesions with AQP4 loss?

To address this question, the sites of T cell infiltration and of AQP4 loss were studied in the following experimental settings: In ENMO induced by MBP-specific T cells, MOG-specific T cells, S100β-specific T cells and two different AQP4-specific T cell lines against the $AQP4_{207\text{-}232}$ and $AQP4_{268–285}$ peptides.

5.2 MBP-specific T cell line

In the first analysis, brain sections from Lewis rats which developed MBP-specific T cell mediated EAE and were then divided into three groups which were injected with 1 ml PBS containing either control IgG (subcuvia), pathogenic NMO IgG J0 or no addition of IgG (Bradl et al 2009). As controls, brain sections from healthy animals without previous T cell treatment, but with injection of either control IgG or NMO IgG J0 (Bradl et al 2009) were also stained, but there was no infiltration of T cells into the brain and no AQP4 loss (data not shown). All animals were sacrificed after 24h after the second injection.

5.2.1 T cell distribution

The distribution pattern of MBP-specific T cells in the brain was comparable in all animals, independently of whether the animals were co-injected with pathogenic NMO IgG J0, control IgG or no IgG at all. Neither the depth of infiltration nor the location of infiltration sites was affected. T cells were observed perivascular and

diffusely within parenchyma. Perivascular cuffs with T cells were mainly found in the cerebellum (Fig. 3b, c) and rarely in the midbrain (Fig. 3a).

At the most prominent infiltration sites the T cells infiltrated the CNS parenchyma via the subpial glia limitans at the basal hypothalamus (Fig. 3d), the third ventricle (Fig. 3e) and fourth ventricle.

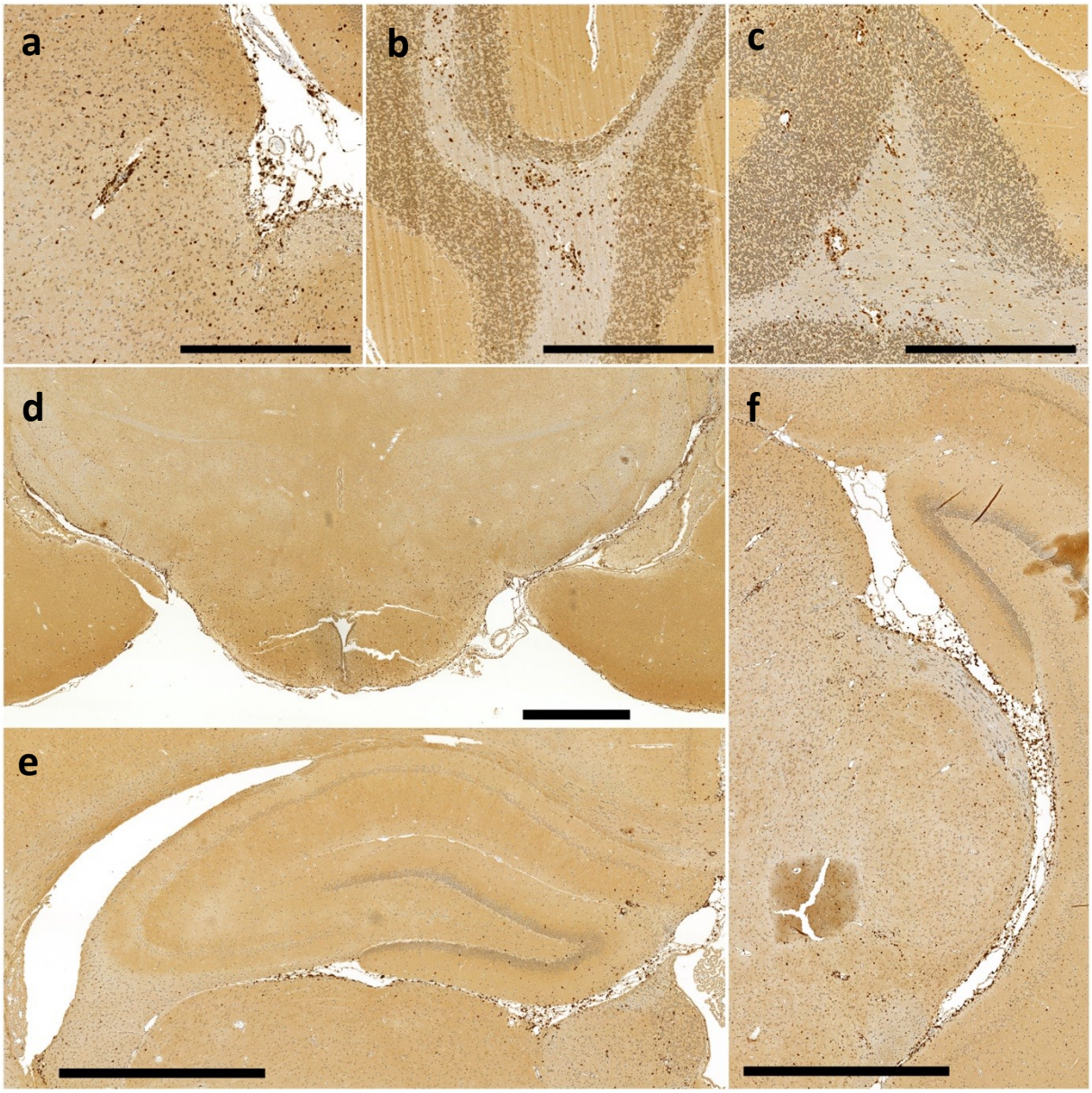

Fig. 3: Brain MBP-specific T cell Infiltration

Perivascular cuffs with T cells in the midbrain (a) and the cerebellum (b, c). Examples of the most prominent T cell infiltration sites at the basal hypothalamus (d), the third ventricle (e) and between hippocampus and the thalamus (f). At the onset of MBP-specific T cell-induced EAE the animals were injected with NMO IgG J0 (a, b, d, e), PBS (c) or control IgG (f) which had no influence on the T cell distribution pattern seen in the brain. The sections were stained with anti-CD3 antibodies to reveal T cells (dark brown). Counterstaining was done for all with haematoxylin to reveal nuclei (blue). Scale bar 500 µm (a-c), 1 mm (d-f)

The areas of CD3-positive T cell infiltration were projected onto schemes (Fig. 4) provided by Paxinos and Watson (Paxinos & Watson 1998).

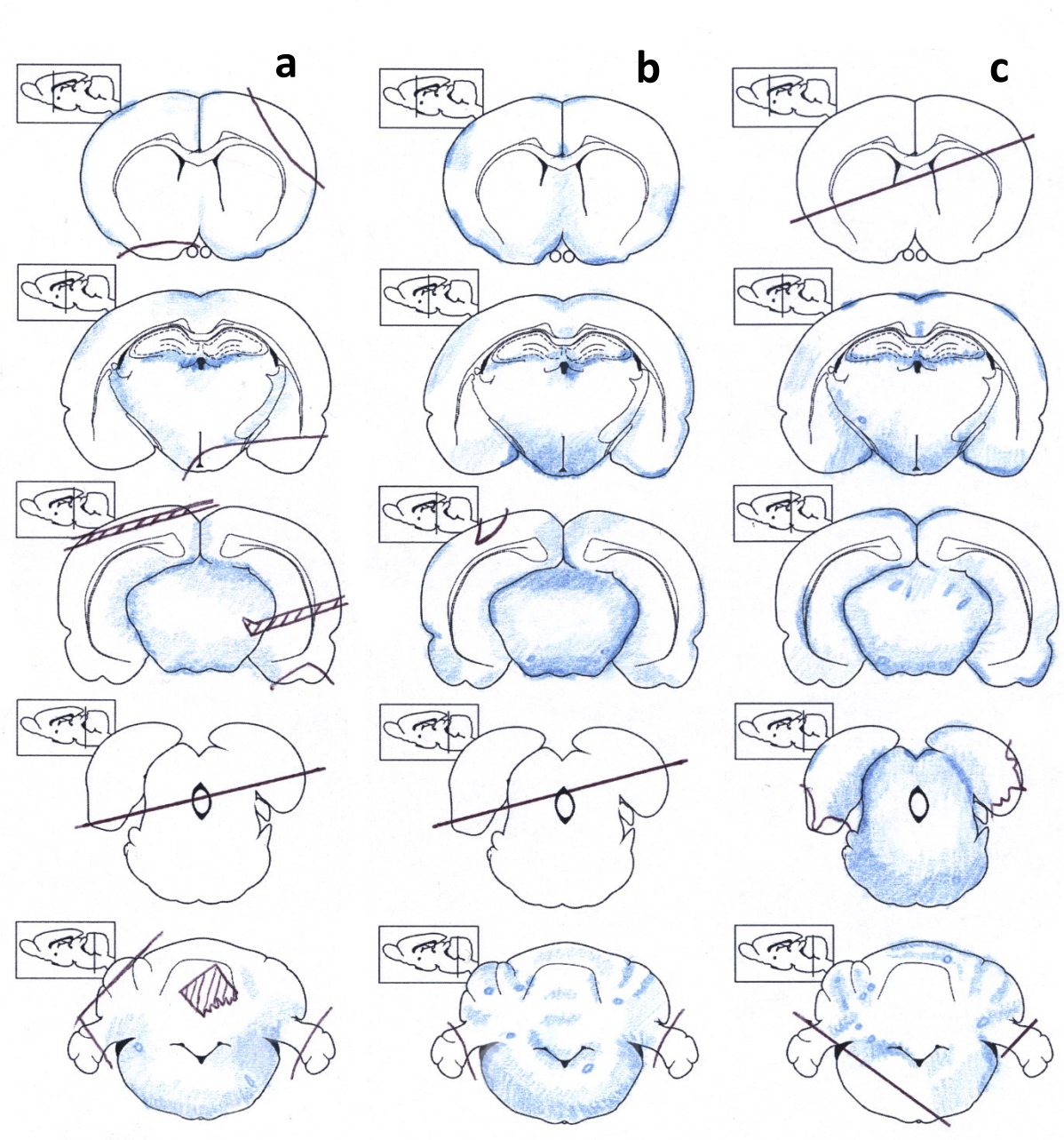

Fig. 4: Distribution of CD3 positive T cells in ENMO rat brain, using schemes provided by Paxinos and Watson (Paxinos & Watson 1998), the animals were treated with MBP-specific T cells and control IgG (a), PBS (b) or NMO IgG J0 (c). The schemes shown are representative for 5 animals/group analysed. White schemes with crossing line: corresponding brain sections were not available and black lines or areas define missing parts.

5.2.2 Lesions with AQP4 loss

Only animals injected with pathogenic NMO IgG J0 at the onset of MBP-specific T cell-induced EAE showed NMO like lesions with AQP4 loss. Lesions with AQP4 loss and increased number of T cells and granulocytes were primarily located at the basal hypothalamus, all over the midbrain (Fig. 5), the medulla and close to the fourth ventricle (Fig. 5e, f). In the cerebellum however only small lesions were found (Fig. 5a, b).

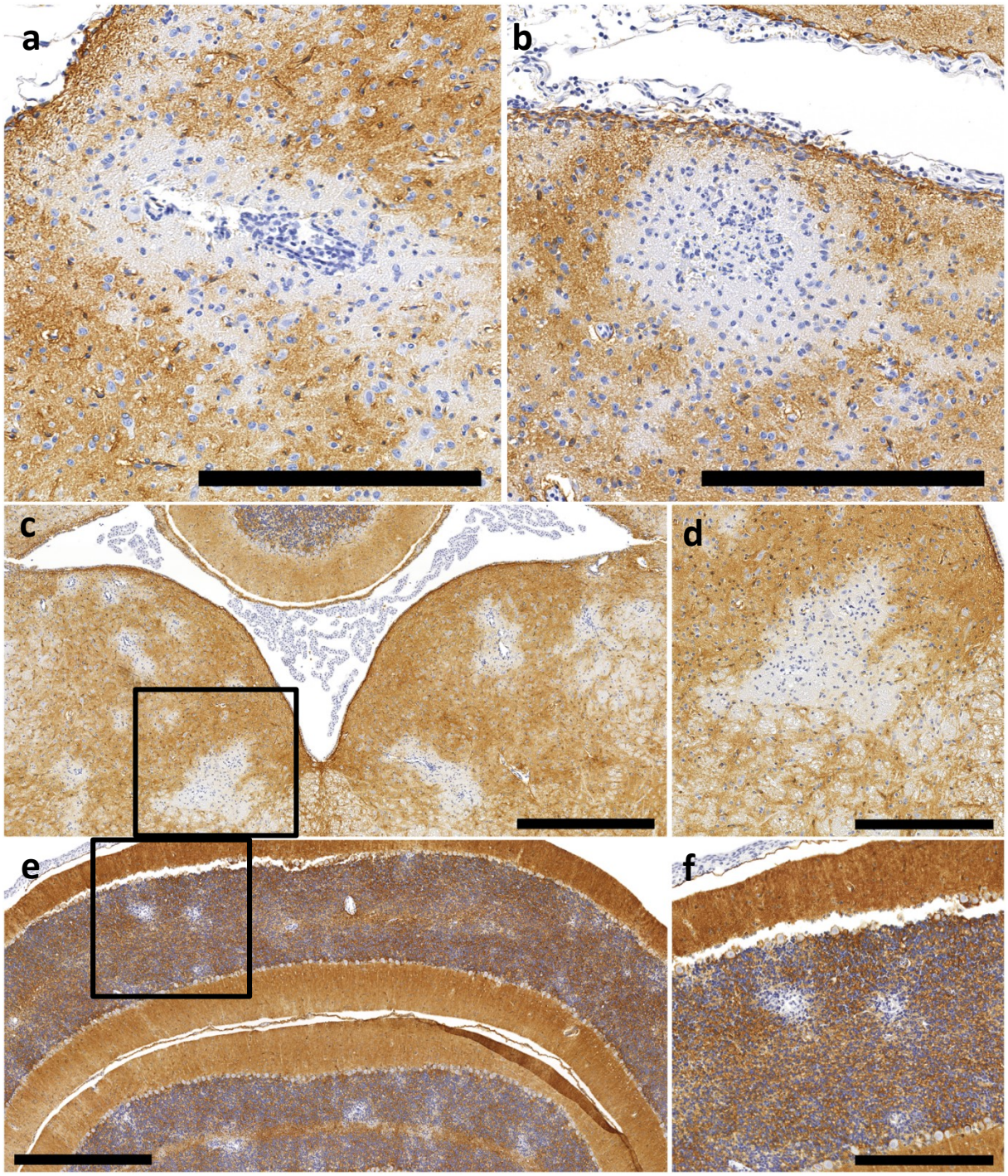

Fig. 5: NMO-like lesions with AQP4 loss of animals injected with pathogenic NMO IgG J0 at the onset of MBP-specific T cell-induced EAE. Large NMO-like lesions with complete AQP4 loss and increase of granulocytes and macrophages were seen in the midbrain (a, b) and close to the forth ventricle and in the medulla (c, d). In the cerebellum only small lesions with distinct AQP4 loss were found (e, f). The sections were stained with anti-AQP4 antibody to show the presence (brown) and the loss (white) of this protein. The counterstaining was done with haematoxylin to reveal nuclei (blue). Scale bar 250 µm (a, b, d, f), 500 µm (a, c, e)

All lesions with AQP4 loss found in five animals injected with MBP-specific T cells and NMO IgG J0 were projected onto schemes (Fig. 6) provided by Paxinos and Watson (Paxinos & Watson 1998).

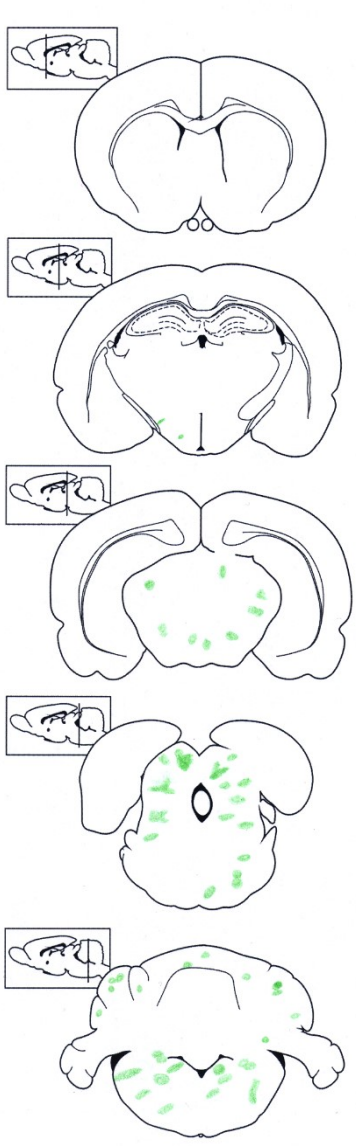

Fig. 6: Loss of AQP4 reactivity in ENMO rat brain, using schemes provided by Paxinos and Watson (Paxinos & Watson 1998). The animals were treated with MBP-specific T cells and NMO IgG J0. The scheme shown is representative for 5 animals analysed.

5.3 MOG-specific T cell line

To further investigate the influence of the specificity of the T cell lines on the T cell distribution and the AQP4 loss in the brain another myelin protein-specific T cell line specific for MOG was used to induce EAE in Lewis rats (Pohl et al 2013). Four days later, the animals then were injected with either NMO IgG J0 or control IgG (Pohl et al 2013) and 24h after antibody injection, the rats were sacrificed and histologically analysed (Pohl et al 2013).

5.3.1 T cell distribution

Independent of injecting pathogenic NMO IgG or control IgG, the animals showed no differences in MOG-specific T cell distribution pattern in the brain. Only a low number of T cells were found within perivascular cuffs (Fig. 7) as compared to animals treated with MBP-specific T cells. Moreover, MOG-specific T cells barely infiltrated into the surrounding tissue. Also at the infiltration sites like basal hypothalamus (Fig. 7c) or third ventricle (Fig. 7f) the T cells stayed at the glia limitans and only few entered the brain parenchyma (Fig. 7).

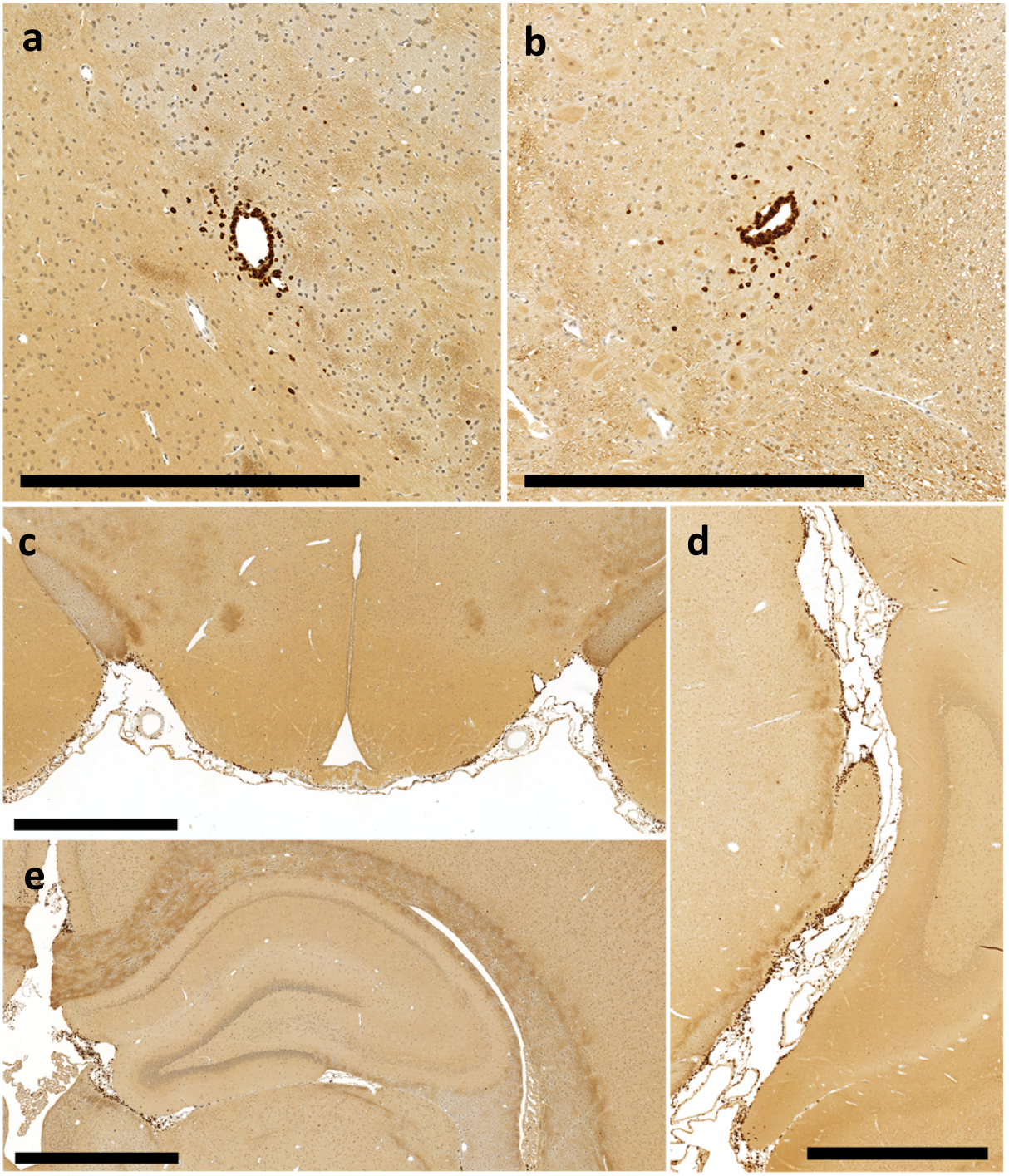

Fig. 7: Brain MOG-specific T cell Infiltration
Perivascular cuffs with T cells in the hypothalamus (a) and medulla (b). Examples of the most prominent T cell infiltration sites at the basal hypothalamus (c), between the thalamus and the hippocampus (d), and at the third ventricle (e). At the onset of MOG-specific T cell-induced EAE the animals were injected with NMO IgG J0 (a, e) or control IgG (b, c, d) which had no influence on the T cell distribution pattern seen in the brain. The sections were stained with anti-CD3 antibodies to reveal T cells (dark brown). Counterstaining was done for all with haematoxylin to reveal nuclei (blue). Scale bar 500 µm (a-b), 1 mm (c-e)

A projection on schemes (Fig. 8) provided by Paxinos and Watson (Paxinos & Watson 1998) for the CD3 positive T cell infiltration was made to give an overview of the pattern.

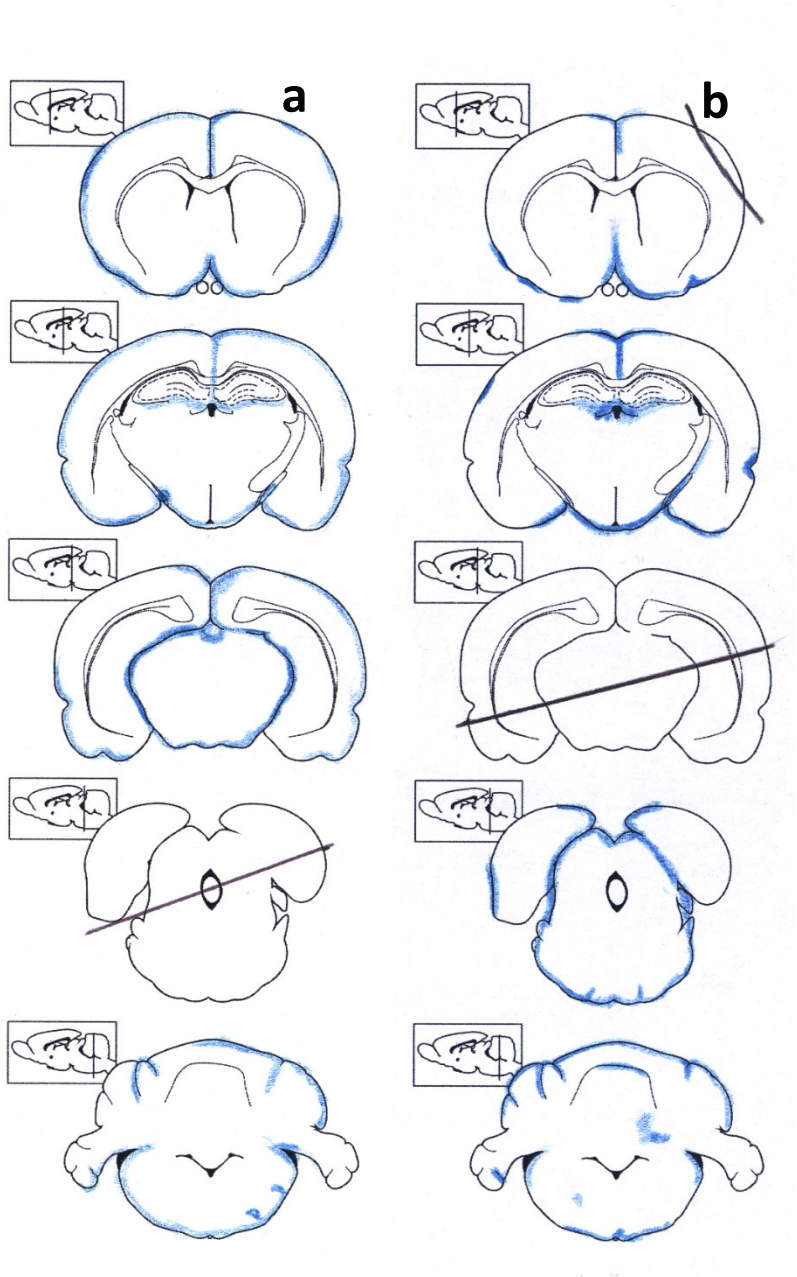

Fig. 8: Distribution of CD3 positive T cells in ENMO rat brain, using schemes provided by Paxinos and Watson (Paxinos & Watson 1998). The animals were treated with (a-b) MOG-specific T cells and NMO IgG J0 (a) or control IgG (b). The schemes shown are representative for 5 animals analysed. White schemes with crossing line: corresponding brain sections were not available and black lines or areas define missing parts.

5.3.2 Lesions with AQP4 loss

Neither the injection of NMO IgG J0 nor control IgG at the onset of MOG-specific T cell-induced EAE caused NMO-like lesions with AQP4 loss.

5.4 S100β-specific T cell line

Lewis rat were co-injected with NMO IgG J0 or control IgG at the onset of S100β-specific T cell-induced EAE (Pohl et al 2013) and 24h later sacrificed. These T cells led to a completely different pathological features in the brain as seen previous in the animals treated with myelin protein-specific T cells.

5.4.1 T cell distribution

The injections with either pathogenic or control IgG hardly affected the amount of S100β-specific T cells infiltrating the brain, only the number of perivascular cuffs containing T cells were slightly elevated in animals injected with pathogenic NMO IgG compared to control animals. The S100β-specific T cells infiltrated the CNS parenchyma via the subpial glia limitans at the third ventricle (Fig. 9d), between the thalamus and the hippocampus (Fig. 9e), the fourth ventricle (Fig. 9f) and lateral fourth ventricle (Fig. 9g).

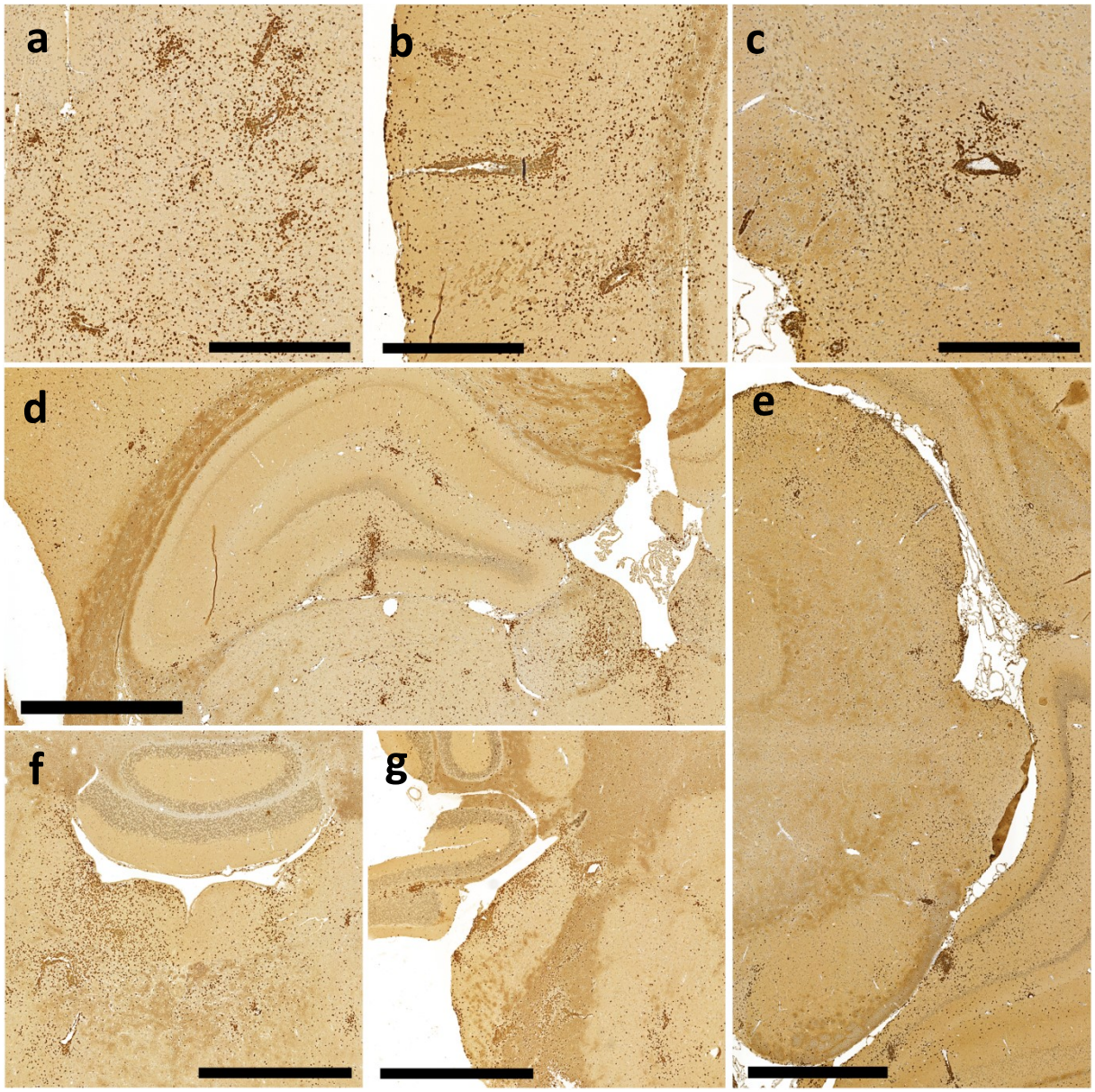

Fig. 9: Brain S100β-specific T cell Infiltration

Cluster of perivascular cuffs with T cells in the midbrain (a), perivascular cuffs containing T cells in the cortex (b) and the hypothalamus (c). Examples of prominent T cell infiltration sites at third ventricle (d), between thalamus and hippocampus (e), fourth ventricle (f) and lateral fourth ventricle (g). At the onset of S100β-specific T cell-induced EAE the animals which were injected with NMO IgG J0 (a, b, d, f, g) or control IgG (c, e) which had no influence on the T cell distribution pattern seen in the brain. The sections were stained with anti-CD3 antibodies to reveal T cells (dark brown). Counterstaining was done for all with haematoxylin to reveal nuclei (blue). Scale bar 500 µm (a-c), 1 mm (d-g)

The CD3 positive T cell distribution in the brain were projected on schemes (Fig. 10) provided by Paxinos and Watson (Paxinos & Watson 1998).

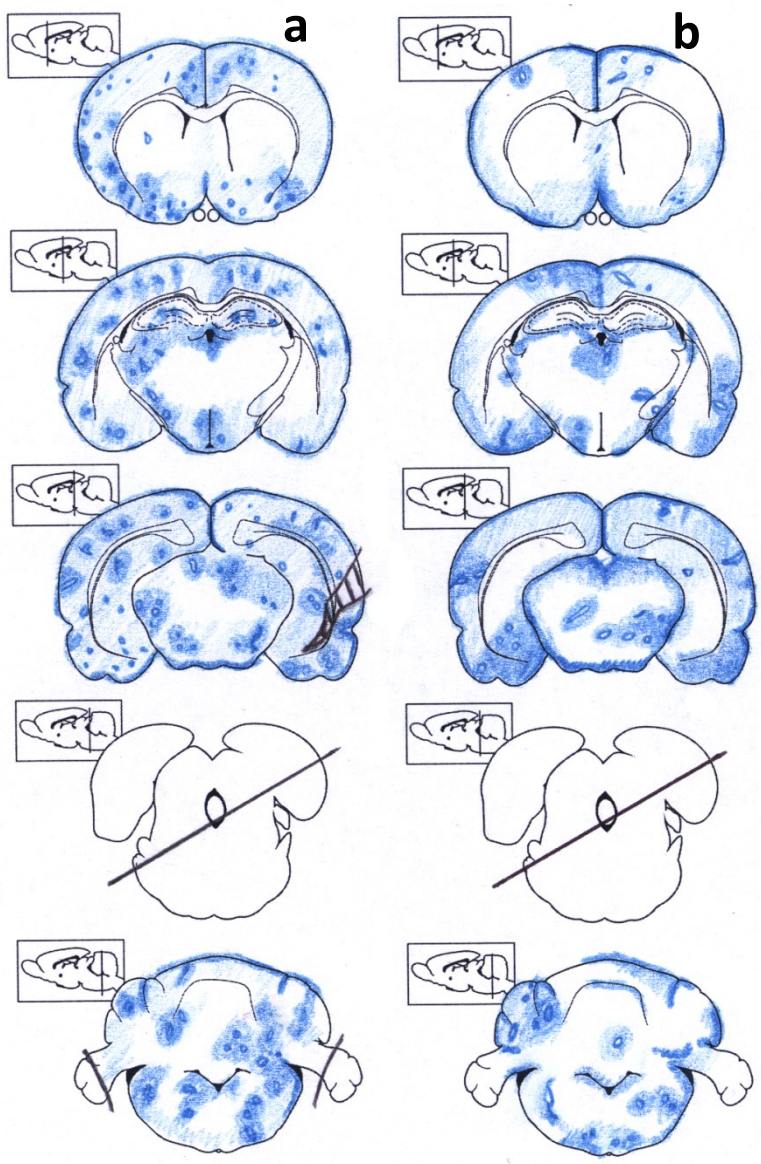

Fig. 10: Distribution of CD3 positive T cells in ENMO rat brain, using schemes provided by Paxinos and Watson (Paxinos & Watson 1998). The animals were treated with S100β-specific T cells and NMO IgG J0 (a) or control IgG (b). The schemes shown are representative for 5 animals analysed. White schemes with crossing line: corresponding brain sections were not available and black lines or areas define missing parts.

5.4.2 Lesions with AQP4 loss

Only the combination of S100β-specific T cells and pathogenic NMO IgG J0 induced NMO-like lesions with AQP4 loss in the brains (Fig. 11). The lesions were distributed throughout the whole brain, except for the cerebellum, where the number was decreased and hippocampus and caudate putamen showed no lesions with AQP4 loss at all.

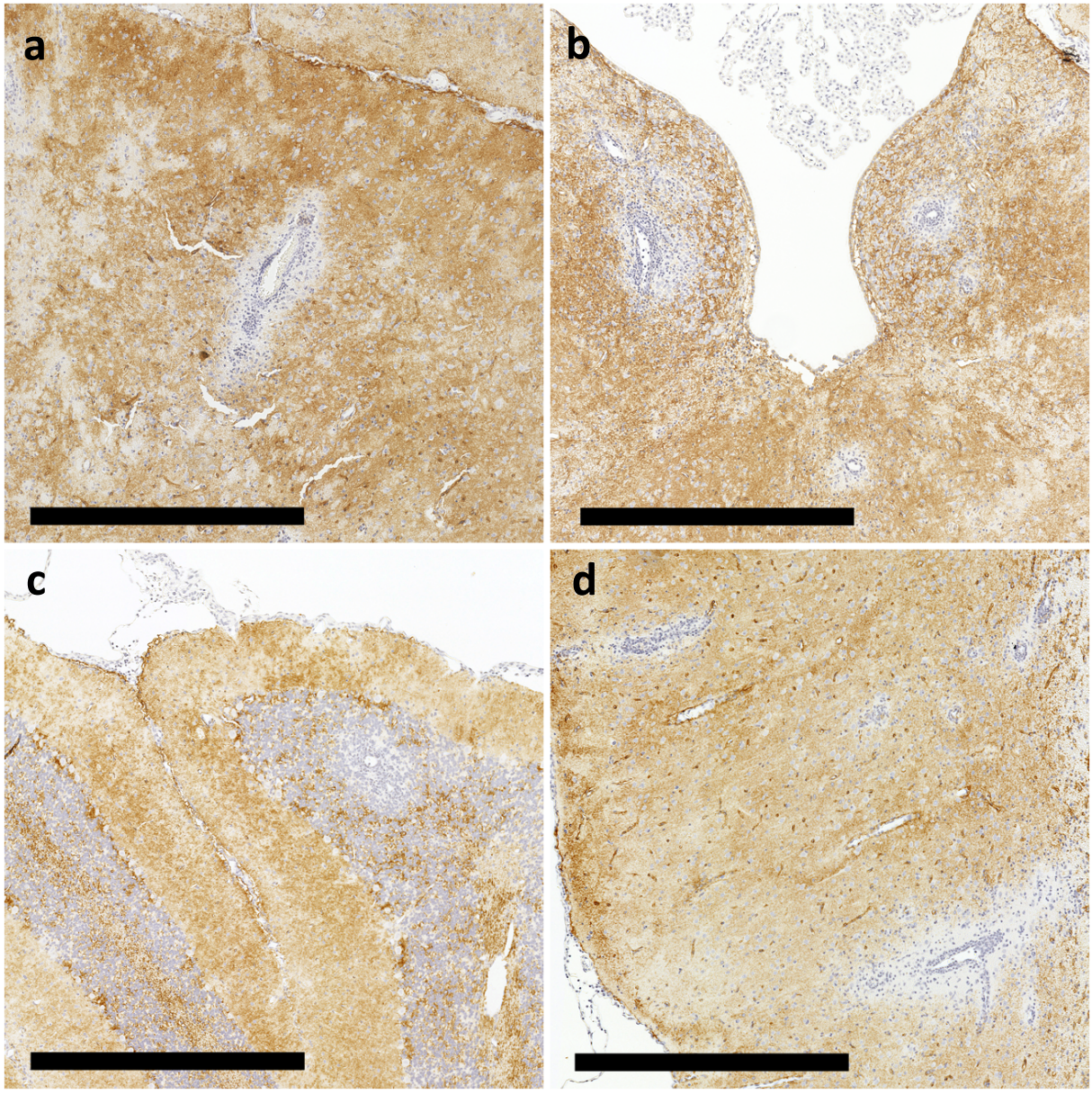

Fig. 11: NMO-like lesions with AQP4 loss of animals injected with pathogenic NMO IgG J0 at the onset of S100β-specific T cell-induced EAE. Large NMO-like lesions with complete AQP4 reactivity loss and increase of granulocytes and macrophages were seen in the whole brain. Examples shown here of lesions in the midbrain (a), close to the third ventricle (b), the cerebellum (c) and in the cortex (d). The sections were stained with anti-AQP4 antibody to show the presence (brown) and the loss (white) of this protein. The counterstaining was done with haematoxylin to reveal nuclei (blue). Scale bar 500 µm

The schemes (Fig. 12) provided by Paxinos and Watson (Paxinos & Watson 1998) were used to project on the NMO-like lesions pattern with AQP4 loss of five animals.

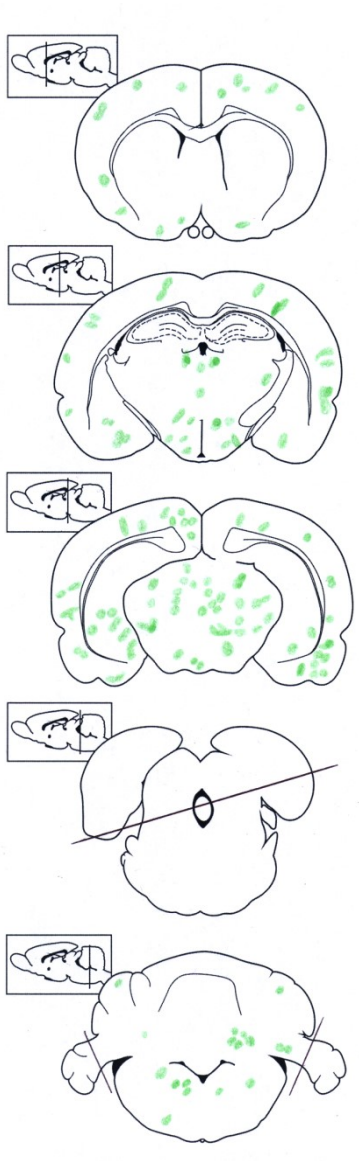

Fig. 12: Loss of AQP4 reactivity in ENMO rat brain, using schemes provided by Paxinos and Watson (Paxinos & Watson 1998). The animals were treated with S100β-specific T cells and NMO IgG J0. The scheme shown is representative for 5 animals analysed. White schemes with crossing line: corresponding brain sections were not available and black lines or areas define missing parts.

5.5 $AQP4_{207-232}$-specific T cell line

Lewis rats were treated with $AQP4_{207-232}$-specific T cells to induce EAE. When the animals showed the first clinical signs of EAE they were injected with NMO IgG J0 or control IgG (Pohl et al 2011) and sacrificed 24h later to investigate the T cell distribution and potential to induce NMO-like lesions with AQP4 loss in the brain.

5.5.1 T cell distribution

Independent of the additional injection with pathogenic NMO IgG or control IgG, at the onset of the $AQP4_{207-232}$-specific T cell-induced EAE, animals showed the same T cell distribution in the brain (Fig. 13). Even though there were sites with increased T cell numbers, the cells seemed to be piled up in the meninges and did not enter the brain parenchyma.

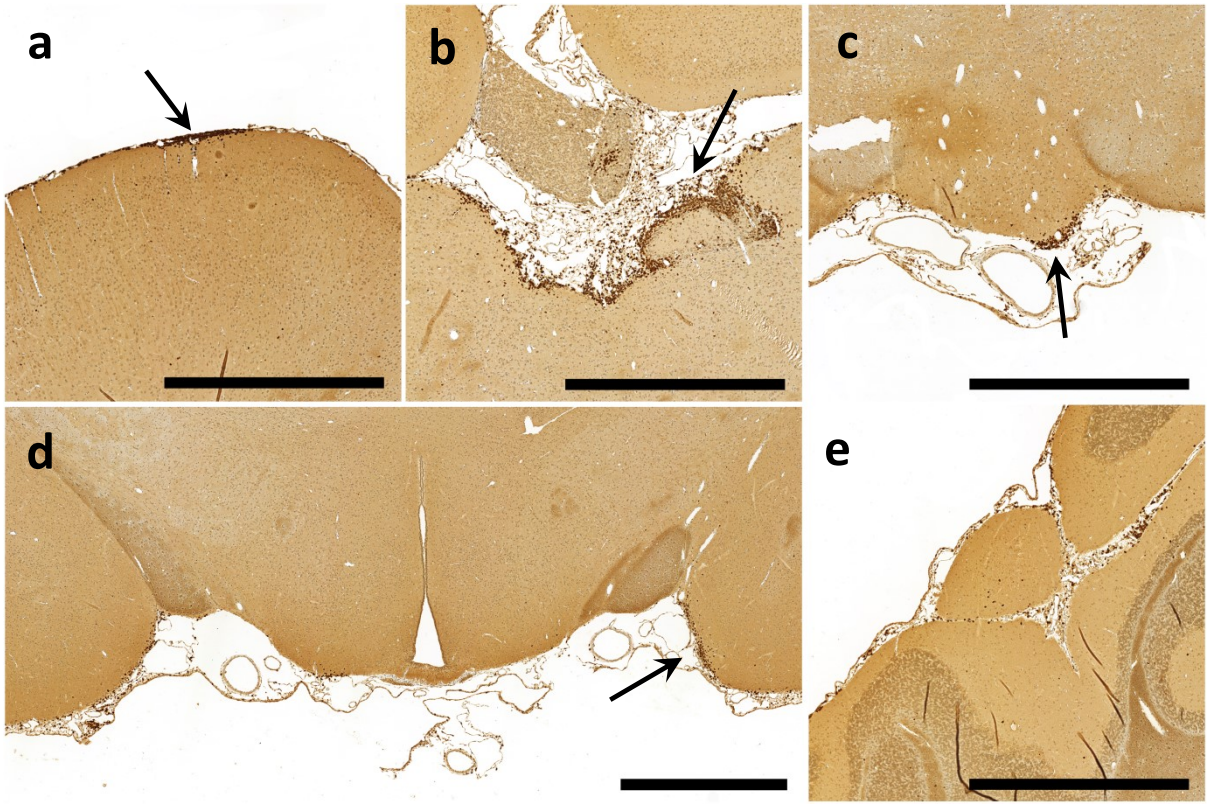

Fig. 13: Brain AQP4$_{207-232}$-specific T cell infiltration
Examples of prominent T cell infiltration sites at the cortex (a), the midbrain (b, c), the basal hypothalamus (d) and the cerebellum (e). T cells are piled up in the meninges (arrows). At the onset of AQP4$_{207-232}$-specific T cell-induced EAE the animals were injected with NMO IgG J0 (a, b, e) or control IgG (c, d). All animals showed similar T cell distribution pattern in the brain. The sections were stained with anti-CD3 antibodies to reveal T cells (dark brown). Counterstaining was done for all with haematoxylin to reveal nuclei (blue). Scale bar 1 mm (a-e)

The CD3 positive T cell distribution in the brain were projected on schemes (Fig. 14) provided by Paxinos and Watson (Paxinos & Watson 1998).

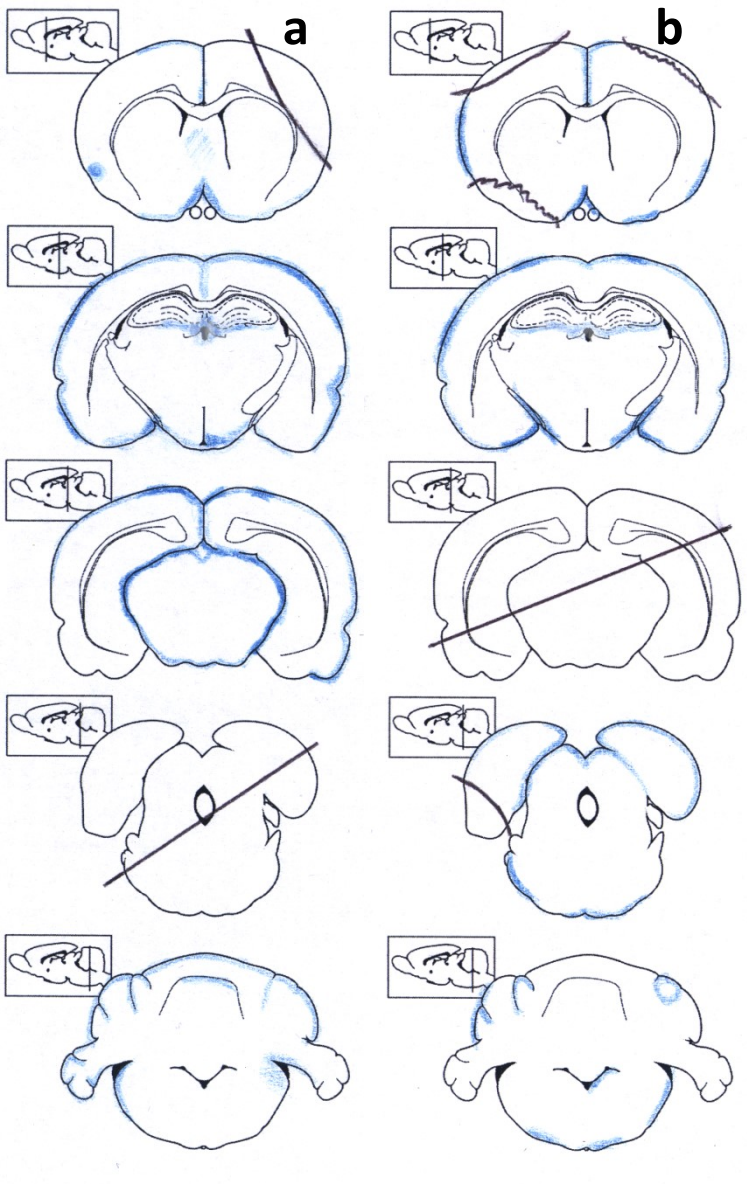

Fig. 14: Distribution of CD3 positive T cells in ENMO rat brains, using schemes provided by Paxinos and Watson (Paxinos & Watson 1998). The animals were treated with (a-b) $AQP4_{207-232}$-specific T cells and NMO IgG J0 (a) or control IgG (b). The schemes shown are representative for three animals analysed. White schemes with crossing line: corresponding brain sections were not available and black lines or areas define missing parts.

5.5.2 Lesions with AQP4 loss

Neither the injection of NMO IgG J0 nor control IgG at the onset of $AQP4_{207-232}$-specific T cell-induced EAE were capable to induce NMO-like lesions with AQP4 loss.

5.6 $AQP4_{268–285}$-specific T cell line

At the onset of $AQP4_{268–285}$-specific T cells (3×10^6) mediated EAE the Lewis rats were injected with NMO IgG9 or control IgG. The animals were sacrificed for further analysis either after 24h or 48h. Additionally, two animals were treated with a higher dose of the $AQP4_{268–285}$-specific T cells (2×10^7) and the same co-injections and sacrificing after 24h. (Zeka et al 2015)

5.6.1 T cell distribution of 3×10^6 injected $AQP4_{268–285}$-specific T cells

The $AQP4_{268–285}$-specific T cells infiltrated the brain parenchyma deeper in animals co-injected with pathogenic NMO IgG compared to the control animals sacrificed at the same time point. The time point also influenced the T cell distribution, the animals showed a higher number of T cells at the infiltration sites after 24h and more extensive T cell distribution than their “counterparts” after 48h. Interestingly, only animals treated with control IgG showed a very high number of perivascular cuffs containing T cells in the cerebellum (Fig. 15a).

At the most prominent infiltration sites, the $AQP4_{268–285}$-specific T cells infiltrated the CNS parenchyma via the subpial glia limitans at the lateral fourth ventricle (Fig. 15b), the fourth ventricle (Fig. 15c), and the third ventricle (Fig. 15d), between the thalamus and the hippocampus (Fig. 15e) and the basal hypothalamus (Fig. 15f).

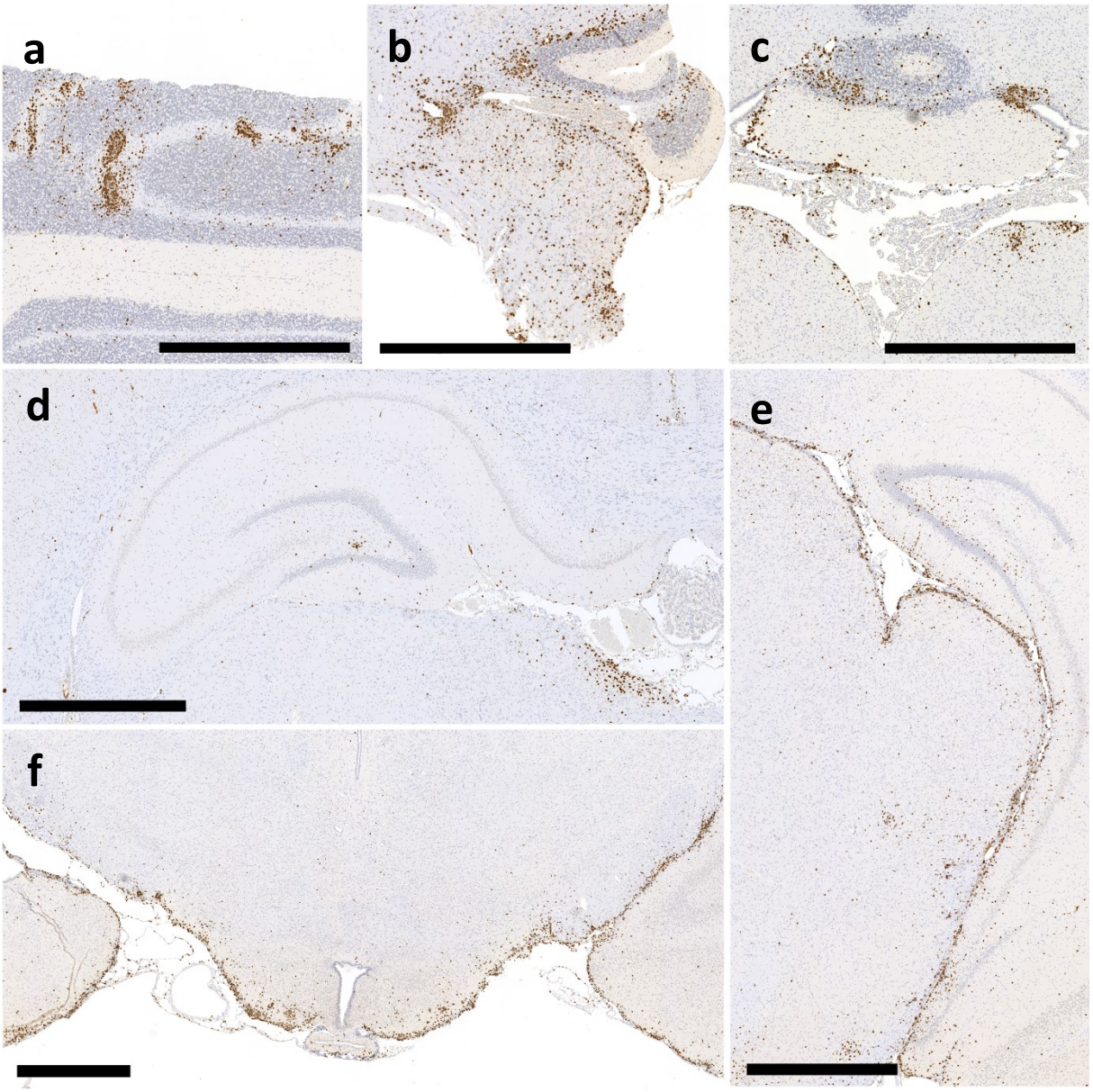

Fig. 15: Brain AQP4$_{268–285}$-specific T cell infiltration

Perivascular cuffs containing T cells in the cerebellum (a). Examples of prominent T cell infiltration sites at the lateral fourth (b), the fourth ventricle (c), third ventricle (d), between the thalamus and the hippocampus (e) and at the basal hypothalamus (f). At the onset of AQP4$_{268–285}$-specific T cell-induced EAE, the animals which were injected with control IgG and sacrificed after 24h (c, f) or 48h (a). Another group of animals received AQP4$_{268–285}$-specific T cells co-injected with NMO IgG9 and were also sacrificed after 24h (b, e) or 48h (d). The sections were stained with anti-CD3 antibodies to reveal T cells (dark brown). Counterstaining was done for all with haematoxylin to reveal nuclei (blue). Scale bar 1 mm (a-f)

The location of the CD3 positive T cells in the brain were projected on schemes (Fig. 16) provided by Paxinos and Watson (Paxinos & Watson 1998)

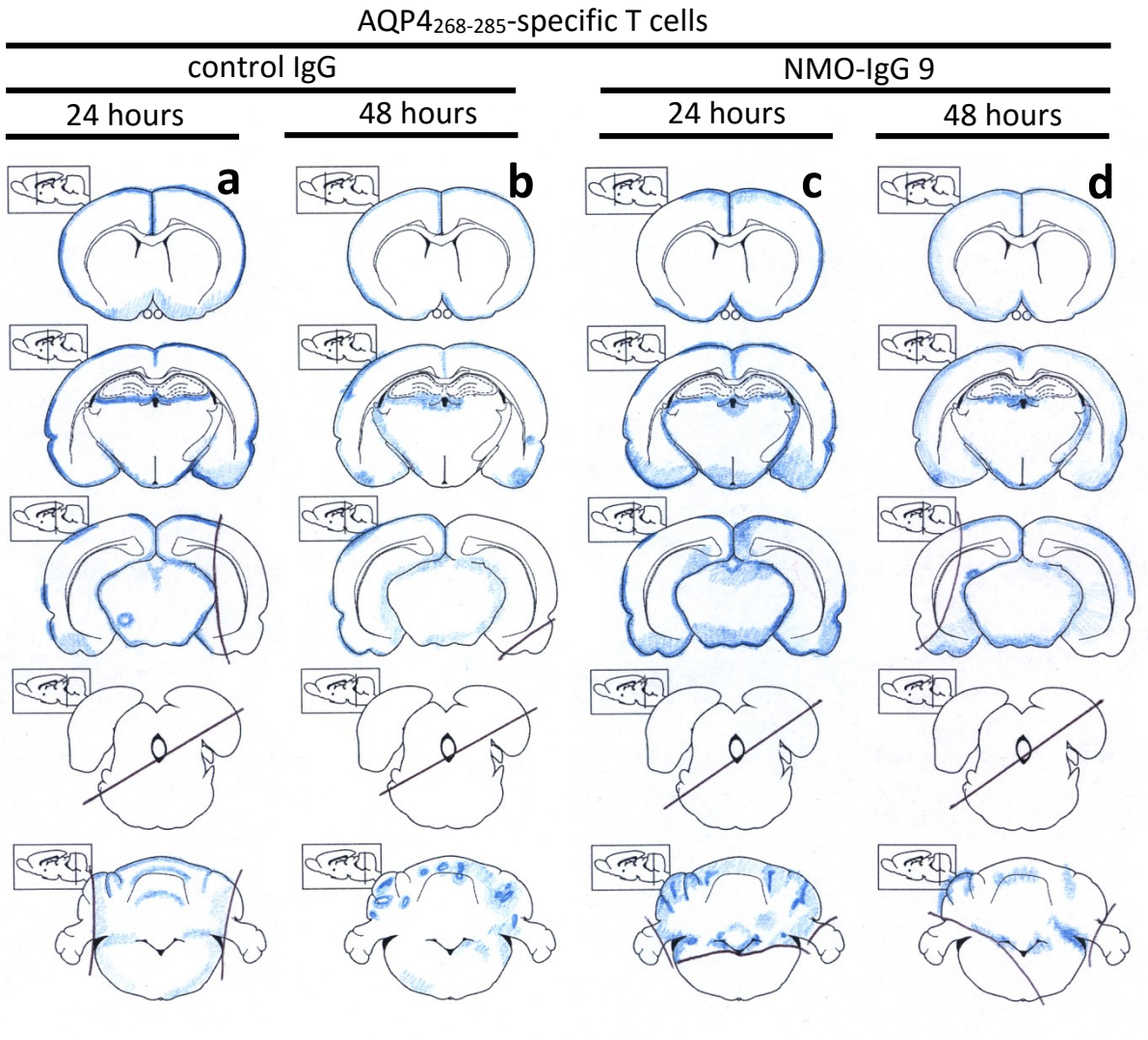

Fig. 16: Distribution of CD3 positive T cells in ENMO rat brains, using schemes provided by Paxinos and Watson (Paxinos & Watson 1998). The animals were treated with $AQP4_{268–285}$-specific T cells (3 x 10^6) and co-injected with control IgG (a, b) or NMO IgG 9 (c, d). The animals were sacrificed after 24h (a, c) or 48h (b, d) after injection with NMO IgG9 or control IgG. The schemes shown are representative for 5 animals analysed. White schemes with crossing line: corresponding brain sections were not available and black lines or areas define missing parts.

5.6.2 T cell distribution of 2 x 10^7 injected $AQP4_{268–285}$-specific T cells

The higher dose of injected $AQP4_{268–285}$-specific T cells (2 x 10^7) led to an increased number of T cells, a more widespread distribution and deeper infiltration of these cells in the brain. Perivascular cuffs containing T cells (Fig. 17a, b, c) were found all

over the whole brain. Infiltration sites of the AQP4$_{268–285}$-specific T cells into the CNS parenchyma were the third ventricle, between the thalamus and the hippocampus (Fig. 17e) and the basal hypothalamus (Fig. 17f).

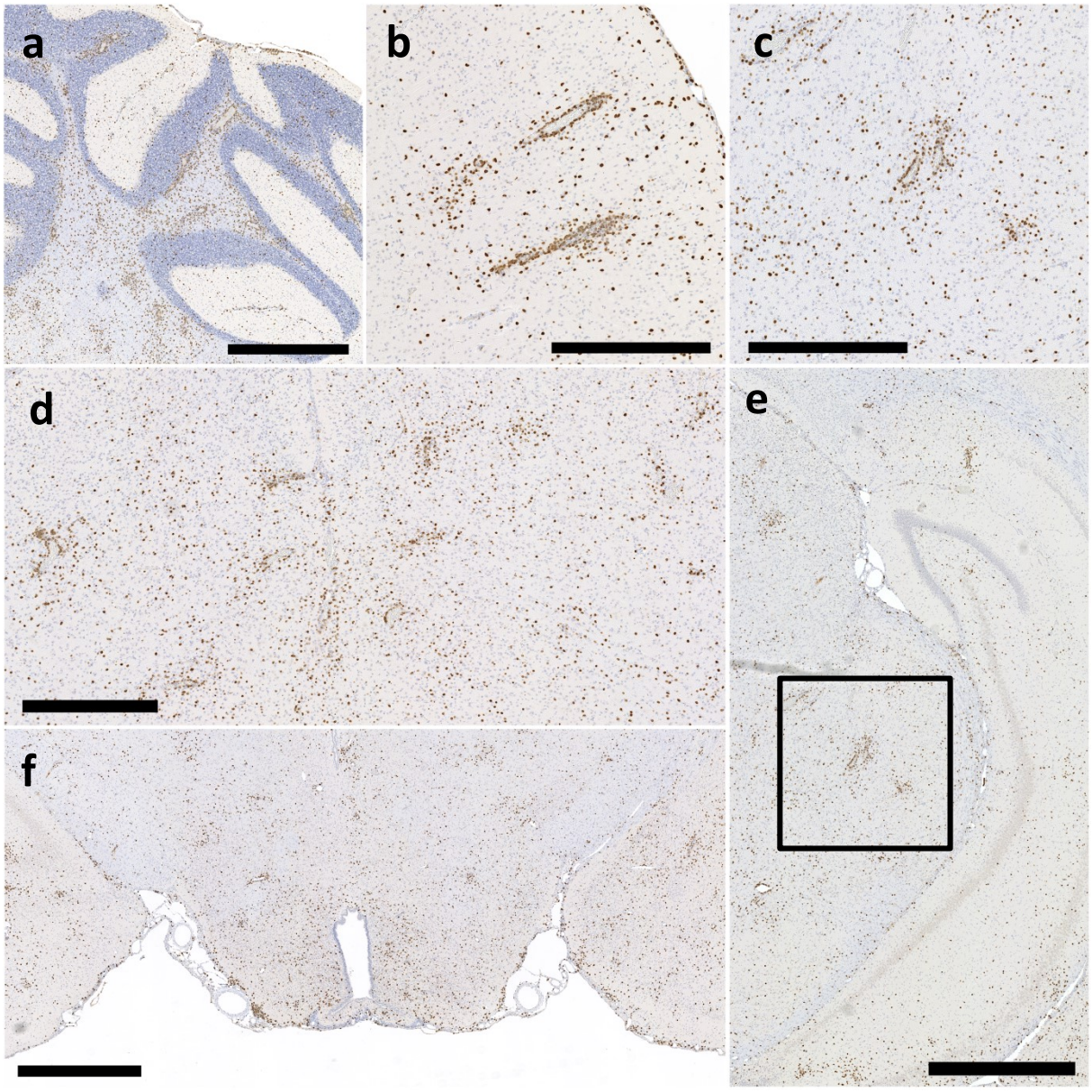

Fig. 17: Brain AQP4$_{268–285}$-specific T cell infiltration higher dosage
Perivascular cuffs with T cells in the cerebellum (a) cortex (b), thalamus (c = box of e) and midbrain (d). Examples of prominent T cell infiltration sites between the thalamus and the hippocampus (e) and at the basal hypothalamus (f). At the onset of AQP4$_{268–285}$-specific T cells (2 x 10^7) induced EAE the animals were injected with NMO IgG IgG9 (a-f) and sacrificed after 24h. The animals showed an increased number of perivascular cuffs filled with T cells and infiltration depth into the brain parenchyma as compared to animals with 3 x 10^6 AQP4$_{268–285}$-specific T cell-injection. The sections were stained with anti-CD3 antibodies to reveal T cells (dark brown). Counterstaining was done for all with haematoxylin to reveal nuclei (blue). Scale bar 500µm (a-d), 1mm (e-f)

On the schemes provided Paxinos and Watson by (Paxinos & Watson 1998) CD3 positive T cell distribution patterns of the brain (Fig. 18) were projected.

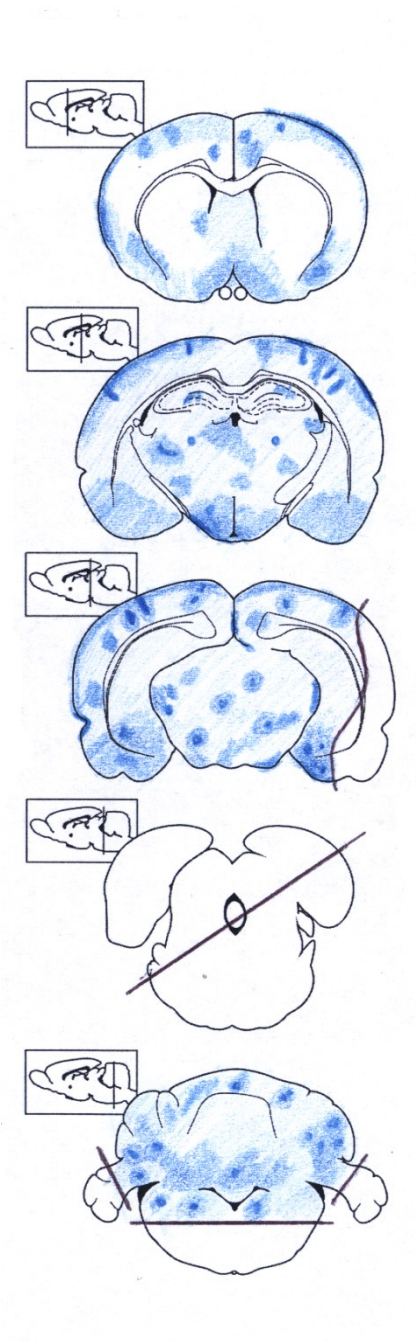

Fig. 18: Distribution of CD3 positive T cells in ENMO rat brain, using schemes provided by Paxinos and Watson (Paxinos & Watson 1998). The animals were treated with $AQP4_{268–285}$-specific T cells (2 x 10^7) and NMO IgG 9 (24h). The schemes shown are representative for two animals analysed. White schemes with crossing line: corresponding brain sections were not available and black lines or areas define missing parts.

5.6.3 Lesions with AQP4 loss

When 3 x 10^6 $AQP4_{268–285}$-specific T cells were used to induce EAE, neither the injection of NMO IgG 9 nor control IgG could to induce NMO-like lesions with AQP4 loss. However, 2 x 10^7 $AQP4_{268–285}$-specific T cells together with NMO IgG 9 initiated a high number of astrocyte-destructive lesions throughout the whole brain after 24h. The larger NMO-like lesions with AQP4 loss were primarily found in the midbrain (Fig. 19a), whereas small lesions appeared in the cortex (Fig. 19b), the thalamus and hypothalamus, as well as cerebellum (Fig. 19c) and medulla (Fig. 19d).

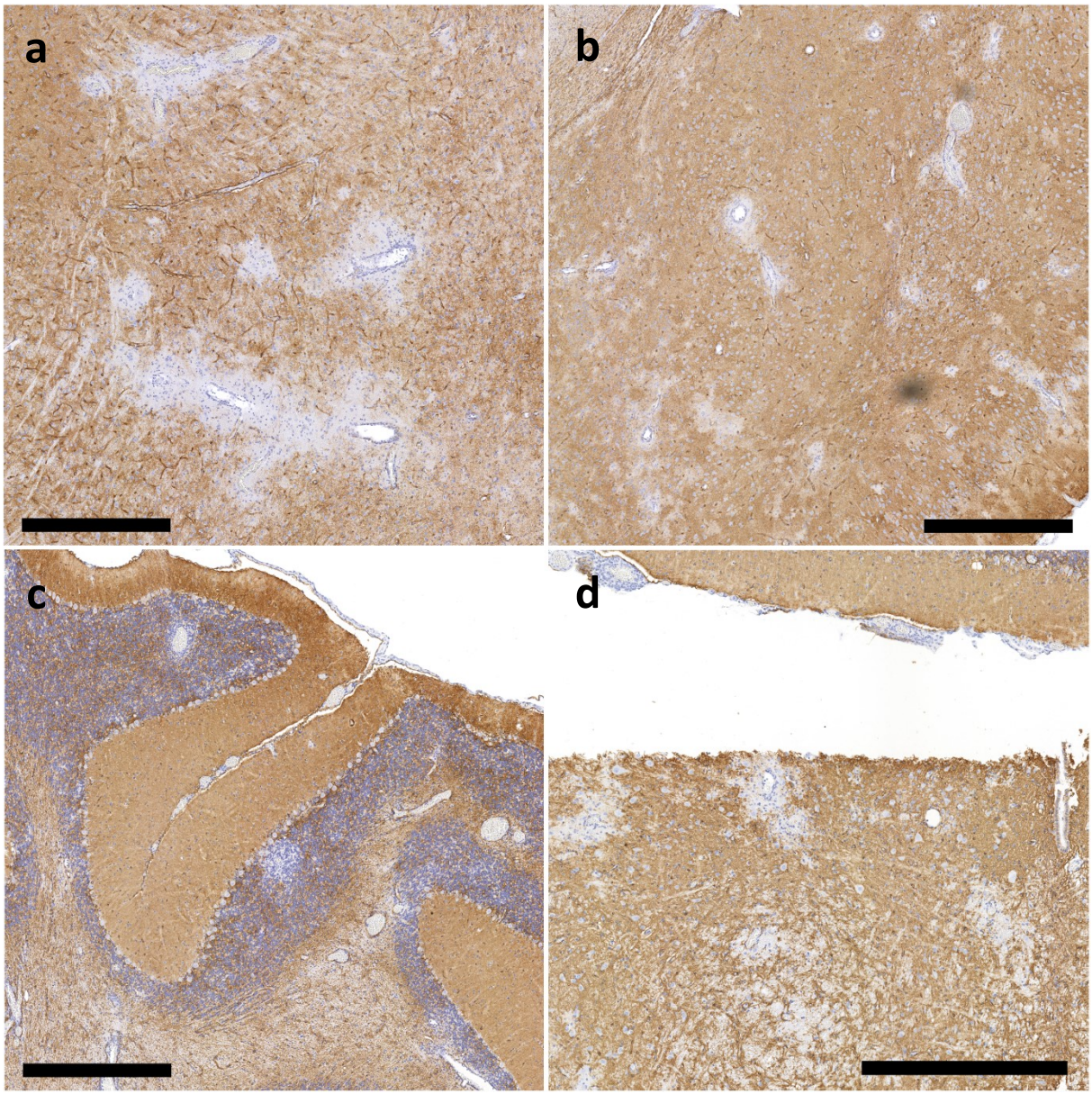

Fig. 19: NMO-like lesions with AQP4 loss of animals injected with pathogenic NMO IgG9 at the onset of AQP4$_{268–285}$-specific T cells (2 x 10^7) induced EAE and sacrificed after 24h after antibody injection. Large NMO-like lesions with complete AQP4 reactivity loss and increase of granulocytes and macrophages were primarily seen. Examples of lesions shown here in the midbrain (a), in the cortex (b), the cerebellum (c) and the medulla (d). The sections were stained with anti-AQP4 antibody to show the presence (brown) and the loss (white) of this protein. The counterstaining was done with haematoxylin to reveal nuclei (blue). Scale bar 500µm

The NMO-like lesions pattern with AQP4 loss (Fig. 20) of two animals were projected on the schemes provided by Paxinos and Watson (Paxinos & Watson 1998).

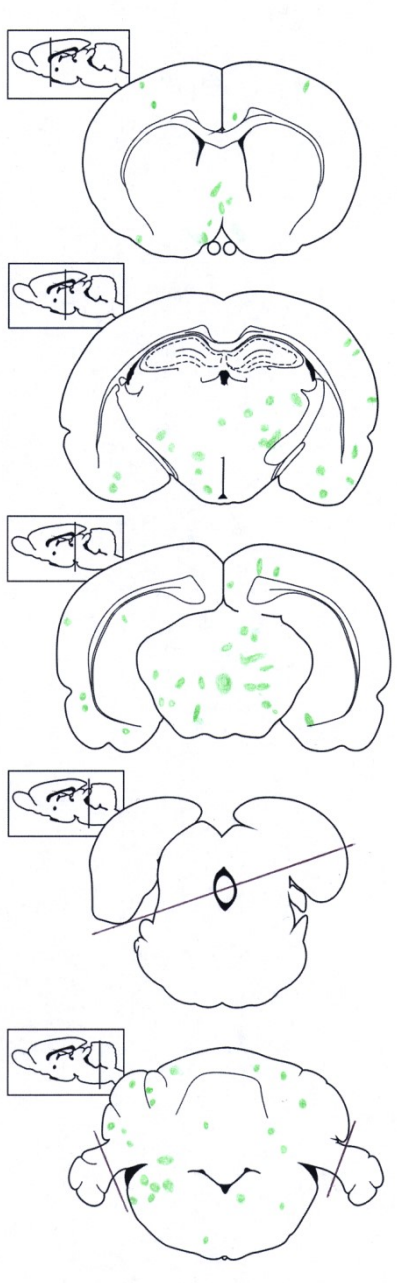

Fig. 20: Loss of AQP4 reactivity in ENMO rat brains, using schemes provided by Paxinos and Watson (Paxinos & Watson 1998). The animals were injected with $AQP4_{268–285}$-specific T cells (2×10^7) when the animals showed first signs of the disease they were injected with NMO IgG9 and sacrificed 24h after second injection. The scheme shown is representative for two animals analysed. White schemes with crossing line: corresponding brain sections were not available and black lines or areas define missing parts.

5.7 Localisation of NMO-like lesions with AQP4 loss

Taken together, only the combination of MBP-specific T cells, S100β-specific T cells and $AQP4_{268–285}$-specific T cells (2×10^7) T cells to induce EAE and co-injection with pathogenic NMO IgGs, when the animals showed the first signs of EAE, led to NMO-like lesions with AQP4 loss in the brain of Lewis rats.

The injection with MBP-specific T cells initiated, compared to the other two T cell lines, a lower number of lesions and they were primarily located all over the midbrain, the medulla and some at the basal hypothalamus (Fig. 21a). In the cerebellum however only small lesions were found (Fig. 21a). Animals injected with S100β-specific T cells however showed the highest number of lesions with AQP4 loss which were distributed all over the brain, only in the cerebellum the number was decreased and the hippocampus and caudate putamen were spared (Fig. 21b). Also $AQP4_{268–285}$-specific T cells led to astrocyte-destructive lesions throughout the whole brain with an increased number of larger lesions in the brainstem (Fig. 21c). For all three animals model the medulla and the brainstem were lesion “hotspots” which is mirroring human NMO.

The lesions with AQP4 loss found in the brains of all animals of each animal model were projected on schemes (Fig. 21) provided by Paxinos and Watson (Paxinos & Watson 1998). Due to the overlay the projected lesion size can be defined by more than one lesion on the same spot in different animals.

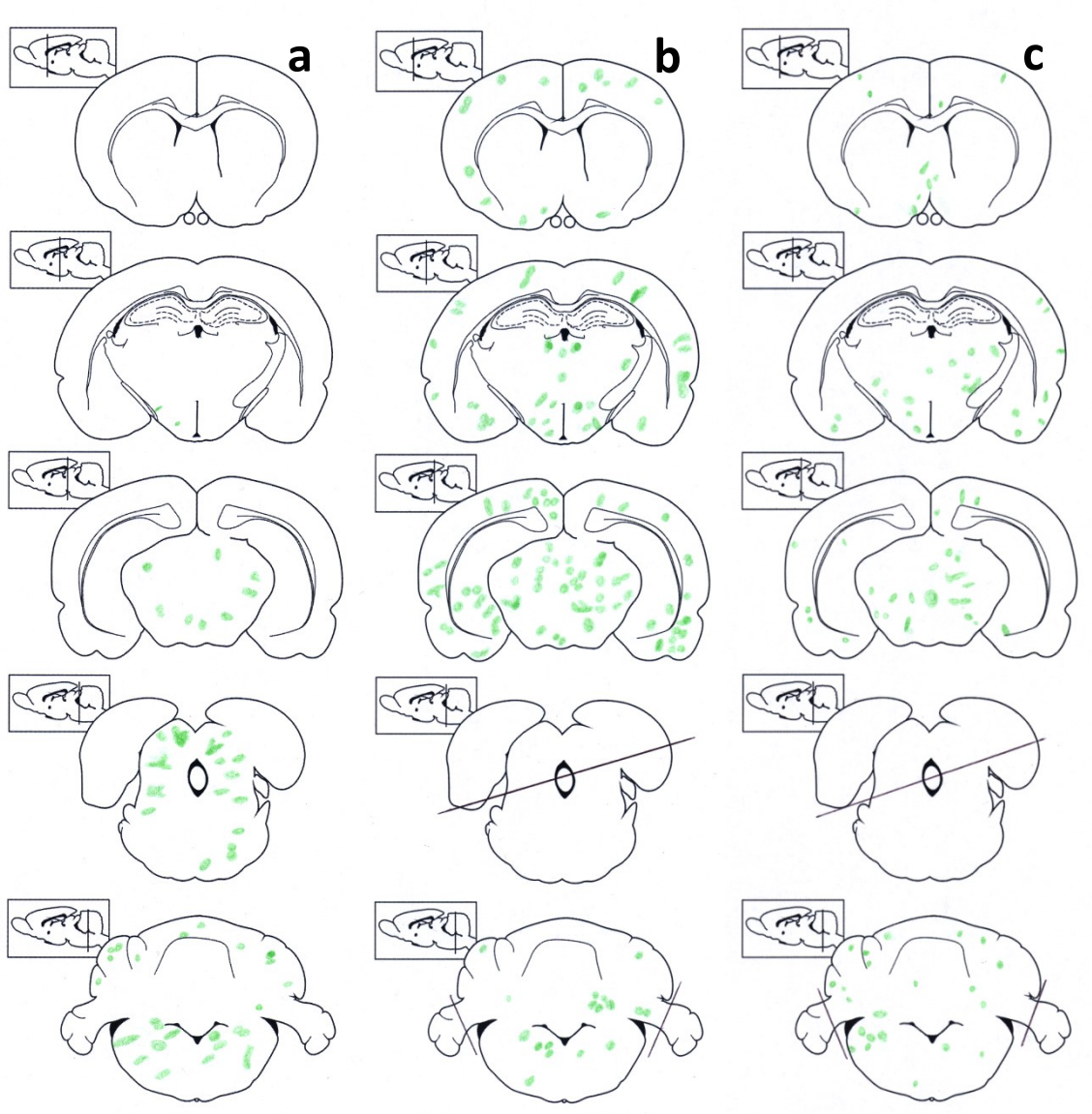

Fig. 21: Loss of AQP4 reactivity in different ENMO rat brains, using schemes provided by Paxinos and Watson (Paxinos & Watson 1998). The animals were treated with T cells to induce EAE and additionally with two different pathogenic NMO IgGs. MBP-specific T cells and NMO IgG J0 (a), S100β-specific T cells and NMO IgG J0 (b) or $AQP4_{268–285}$-specific T cells (2×10^7) and NMO IgG 9. The scheme shown is representative for five animals (a, b) or two animals (c) analysed. White schemes with crossing line: corresponding brain sections were not available and black lines or areas define missing parts.

6. Discussion

This study investigated the pathological features in the brain of NMO animal models using archived material and immunohistochemistry. For NMO animal models, T cell lines specific for different CNS peptides were used, resulting in a variety of pathological features which were partially strikingly similar to NMO in humans. The questions arose whether the location of NMO-like lesions in the brain is determined by the T cell specificity used or a higher vulnerability for the formation of NMO-like lesions in certain areas of the brain?

To address this question, T cell lines with five different peptide-specificities (MBP, MOG, S100β, $AQP4_{207-232}$, $AQP4_{268-285}$) were used to induce EAE in Lewis rats. When the animals showed the first signs of EAE, they were injected with two different pathogenic NMO IgGs (NMO IgG J0, NMO IgG 9) or with control IgG (Bradl et al 2009, Pohl et al 2011, Pohl et al 2013, Zeka et al 2015) to initiate NMO-like lesions with AQP4 loss in the brain.

Independent of the CNS peptide specificity of the T cells, they invaded the brain at the same infiltration sites: the third ventricle, the basal hypothalamus, between thalamus and hippocampus and the fourth ventricle. This correlates with previous results (Berger et al 1997). In order to induce inflammation in the brain and develop EAE, the injected CNS-specific T cells needed to be reactivated via MHC II+ complex and their respective CNS antigens on APC located in the CNS (Kivisakk et al 2009). And indeed, beside the CNS derived proteins which drain from the CNS interstitial fluid into the CSF (Berger et al 1997, Cserr & Knopf 1992) also mature dendritic cells are found in the leptomeninges which have the ability to present antigens to the infiltrating T cells (Kivisakk et al 2009). As seen before (Berger et al 1997, Kivisakk et al 2009) the inflammation starts for all T cells, independent of their specificity, in the meninges and the perivascular space but only MBP-specific T cells, S100β-specific

T cells and $AQP4_{268-285}$-specific T cells, showed the ability to distribute from there into the brain parenchyma. The pathogenicity of T cells-specific for different CNS antigens depends on the degree of reactivation in the CNS (Kawakami et al 2004, Kivisakk et al 2009). Only full reactivation of the T cells leads to upregulation of the expression of pro-inflammatory cytokines and chemokines in the brain and further to the recruitment of activated microglia/macrophages and finally to clinical disease in the animals (Kawakami et al 2004). It was shown that the inflammatory environment additionally influences the location of inflammation in the CNS but the responsible mechanisms are not well understood yet (Pierson et al 2012). The degree of reactivation is determined by the local concentration of the respective antigens and their ability to diffuse into the perivascular and meningeal space (Berger et al 1997, Kawakami et al 2004) as well as the affinity of the peptide/ MHC II complex to T cell receptor (TCR) and also the local cytokine milieu (Kawakami et al 2004). The different activation degrees of the five T cell lines were reflected in their T cell distribution pattern seen in the brain of the animals.

The weakly activated T cells-specific for MOG and $AQP4_{207-232}$ did not infiltrate the brain parenchyma and only few T cells were found in perivascular cuffs. These T cells did not cause any clinical symptoms, as a result of a low production of INF-y and the decreased recruitment of activated microglia/macrophages to the inflammation sites (Linington et al 1993, Pohl et al 2013, Zeka et al 2015) compared to fully activated T cells.

The S100β-specific T cells showed a medium activation and a very high number of T cells infiltrated the brain prarenchyma. S100β is an astrocytic protein and the pia limitans is enriched in astrocytic processes where the antigen could be liberated into the perivascular and meningeal space or directly presented to the T cell (Fontana et al 1984) which could be the reason for the high number of T cells found in the perivascular cuffs. Even though these T cells led to a strong inflammatory response, they were unable to induce a severe disease which was associated with a lower

number of recruited activated microglia/macrophages (Kojima et al 1997, Pohl et al 2013).

The MBP-specific T cells and $AQP4_{268-285}$-specific T cells were fully reactivated in the CNS leading to production of IFN-y and other pro-inflammatory mediators resulting in an increased recruitment of activated microglia/macrophages and severe neurological deficiency in the animals (Berger et al 1997, Pohl et al 2013, Zeka et al 2015). Both T cell lines infiltrated the deep parenchyma and similar to the S100β astrocytic peptide, $APQ4_{268-285}$-specific T cells were increased in the perivascular cuffs.

Even though all five used T cell lines irrespective of their pathogenic potential could render the BBB endothelium permissive for T cell infiltration, only MBP-specific T cells, S100β-specific T cells and $AQP_{268-285}$-specific T cells were sufficiently activated to induce brain lesions with AQP4 loss in combination with a pathogenic NMO IgG.
These NMO-like lesions found in the animals contained T cells, activated microglia/macrophages and granulocytes in striking resemblance to NMO lesions seen in humans. Only the increased number of eosinophils found in humans was not present (Correale & Fiol 2004, Lucchinetti et al 2002) which may be due to the used rat strain (Bradl et al 2009).

It is well known for autoantibodies like NMO IgGs that the antigen specificity of the T cells is irrelevant for them to become pathogenic (Kornek & Lassmann 1999, Linington et al 1988). To initiate NMO-like lesions with AQP4 loss, the T cells are predominantly needed to open the BBB, to induce the inflammation and for the recruitment of activated effector cells like macrophages (Vass et al 1992) to the brain areas where the antigen AQP4 is present (Kornek & Lassmann 1999, Linington et al 1988).

Astrocyte-destructive lesions were found in animals treated with MBP-specific T cells with NMO IgG J0 primarily at the basal hypothalamus, in the midbrain and the

medulla. Animals treated with S100β-specific T cells with NMO IgG J0 showed NMO-like lesions distributed all over the brain, only the hippocampus and caudate putamen where spared. The combination of $AQP4_{268-285}$-specific T cells with NMO IgG 9 also induced lesions in the whole brain, but the midbrain clearly was the "hotspot" for the larger lesions.

Even though the animal model resembles pathological features of the human NMO disease, particularly the situation in the spinal cord, the topography of lesions found in the animal brains did not completely reflect the situation seen in human NMO patients. The most characteristic sites for brain lesions in NMO patients are close to the ventricular system, surrounding the third and fourth ventricle and the aqueduct of Sylvius mirroring the perivascular/hypothalamic localisation of AQP4 (Pittock et al 2006b). Lesions in the brainstem and hypothalamus appear to be typical and also the corpus callosum is sometimes involved (Nakashima et al 2006, Pittock et al 2006a, Poppe et al 2005). The three animal models showed lesions and inflammation at the same sites as NMO patients, but also in "untypical" areas such as the cortex and the cerebellum.

This study reinforced the crucial role of the T cell specificity, in NMO-like lesion distribution in the brain of ENMO models. However, further investigation is needed to understand the fundamental regulating mechanisms of autoimmunity in the CNS and to identify the targeted antigen of the T cells initiating inflammation leading to astrocyte-destructive lesions in the brain, to establish an even more representative animal model.

7. List of abbreviations

APC = antigen presenting cells

AQP4 = aquaporin 4

BBB = blood brain barrier

CNS = central nervous system

CSA = catalysed Signal Amplification

DAB = 3,3’ diaminobenzidine-tetrahydrochloride

EAE = experimental autoimmune encephalomyelitis

ENMO = experimental autoimmune neuromyelitis optica

FCS = fetal calf serum

Ig = immunoglobulin

IgG = immunoglobulin G

MBP = myelin basic protein

MOG = myelin oligodendrocyte glycoprotein

MRI = magnetic resonance images

NMO = euromyelitis optica

OAP = orthogonal arrays of particles

PBS = phosphate buffered saline

PFA = phosphate-buffered paraformaldehyde

TBS =tris-buffered saline

TCR = T cell receptor

ZNS = zentrales Nervensystems

8. List of tables

9. List of figures

Ich habe mich bemüht, sämtliche Inhaber der Bildrechte ausfindig zu machen und ihre Zustimmung zur Verwendung der Bilder in dieser Arbeit eingeholt. Sollt dennoch eine Urheberrechtsverletzung bekannt werden, ersuche ich um Meldung bei mir.

10. References

Aboul-Enein F, Bauer J, Klein M, Schubart A, Flugel A, et al. 2004. Selective and antigen-dependent effects of myelin degeneration on central nervous system inflammation. *Journal of neuropathology and experimental neurology* 63: 1284-96

Adelmann M, Wood J, Benzel I, Fiori P, Lassmann H, et al. 1995. The N-terminal domain of the myelin oligodendrocyte glycoprotein (MOG) induces acute demyelinating experimental autoimmune encephalomyelitis in the Lewis rat. *Journal of neuroimmunology* 63: 17-27

Apiwattanakul M, Popescu BF, Matiello M, Weinshenker BG, Lucchinetti CF, et al. 2010. Intractable vomiting as the initial presentation of neuromyelitis optica. *Annals of neurology* 68: 757-61

Ben-Nun A, Wekerle H, Cohen IR. 1981. The rapid isolation of clonable antigen-specific T lymphocyte lines capable of mediating autoimmune encephalomyelitis. *European journal of immunology* 11: 195-9

Bennett JL, Lam C, Kalluri SR, Saikali P, Bautista K, et al. 2009. Intrathecal pathogenic anti-aquaporin-4 antibodies in early neuromyelitis optica. *Annals of neurology* 66: 617-29

Berger T, Weerth S, Kojima K, Linington C, Wekerle H, Lassmann H. 1997. Experimental autoimmune encephalomyelitis: the antigen specificity of T lymphocytes determines the topography of lesions in the central and peripheral nervous system. *Laboratory investigation; a journal of technical methods and pathology* 76: 355-64

Bradl M, Misu T, Takahashi T, Watanabe M, Mader S, et al. 2009. Neuromyelitis optica: pathogenicity of patient immunoglobulin in vivo. *Annals of neurology* 66: 630-43

Coligan J. 1991. Current protocols in immunology. *Somerset, NJ:*
Wiley

Correale J, Fiol M. 2004. Activation of humoral immunity and eosinophils in neuromyelitis optica. *Neurology* 63: 2363-70

Crane JM, Lam C, Rossi A, Gupta T, Bennett JL, Verkman AS. 2011. Binding affinity and specificity of neuromyelitis optica autoantibodies to aquaporin-4 M1/M23 isoforms and orthogonal arrays. *The Journal of biological chemistry* 286: 16516-24

Cree BA, Goodin DS, Hauser SL. 2002. Neuromyelitis optica. *Seminars in neurology* 22: 105-22

Cserr HF, Knopf PM. 1992. Cervical lymphatics, the blood-brain barrier and the immunoreactivity of the brain: a new view. *Immunology today* 13: 507-12

de Seze J. 2003. Neuromyelitis optica. *Archives of neurology* 60: 1336-8

de Seze J, Lebrun C, Stojkovic T, Ferriby D, Chatel M, Vermersch P. 2003. Is Devic's neuromyelitis optica a separate disease? A comparative study with multiple sclerosis. *Multiple sclerosis* 9: 521-5

Flanagan EP, Weinshenker BG. 2014. Neuromyelitis optica spectrum disorders. *Current neurology and neuroscience reports* 14: 483

Fontana A, Fierz W, Wekerle H. 1984. Astrocytes present myelin basic protein to encephalitogenic T-cell lines. *Nature* 307: 273-6

Fu D, Lu M. 2007. The structural basis of water permeation and proton exclusion in aquaporins. *Molecular membrane biology* 24: 366-74

Fujihara K, Misu T, Nakashima I, Takahashi T, Bradl M, et al. 2012. Neuromyelitis optica should be classified as an astrocytopathic disease rather than a demyelinating disease. *Clinical and Experimental Neuroimmunology* 3: 58-73

Furman CS, Gorelick-Feldman DA, Davidson KG, Yasumura T, Neely JD, et al. 2003. Aquaporin-4 square array assembly: opposing actions of M1 and M23 isoforms. *Proceedings of the National Academy of Sciences of the United States of America* 100: 13609-14

Gonen T, Walz T. 2006. The structure of aquaporins. *Quarterly reviews of biophysics* 39: 361-96

Hinson SR, Pittock SJ, Lucchinetti CF, Roemer SF, Fryer JP, et al. 2007. Pathogenic potential of IgG binding to water channel extracellular domain in neuromyelitis optica. *Neurology* 69: 2221-31

Hinson SR, Romero MF, Popescu BF, Lucchinetti CF, Fryer JP, et al. 2012. Molecular outcomes of neuromyelitis optica (NMO)-IgG binding to aquaporin-4 in astrocytes. *Proceedings of the National Academy of Sciences of the United States of America* 109: 1245-50

Iorio R, Fryer JP, Hinson SR, Fallier-Becker P, Wolburg H, et al. 2013. Astrocytic autoantibody of neuromyelitis optica (NMO-IgG) binds to aquaporin-4 extracellular loops, monomers, tetramers and high order arrays. *Journal of autoimmunity* 40: 21-7

Ishizu T, Osoegawa M, Mei FJ, Kikuchi H, Tanaka M, et al. 2005. Intrathecal activation of the IL-17/IL-8 axis in opticospinal multiple sclerosis. *Brain : a journal of neurology* 128: 988-1002

Kawakami N, Lassmann S, Li Z, Odoardi F, Ritter T, et al. 2004. The activation status of neuroantigen-specific T cells in the target organ determines the clinical outcome of autoimmune encephalomyelitis. *The Journal of experimental medicine* 199: 185-97

King G, Payne S, Walker F, Murray GI. 1997. A highly sensitive detection method for immunohistochemistry using biotinylated tyramine. *The Journal of pathology* 183: 237-41

Kivisakk P, Imitola J, Rasmussen S, Elyaman W, Zhu B, et al. 2009. Localizing central nervous system immune surveillance: meningeal antigen-presenting cells activate T cells during experimental autoimmune encephalomyelitis. *Annals of neurology* 65: 457-69

Kojima K, Wekerle H, Lassmann H, Berger T, Linington C. 1997. Induction of experimental autoimmune encephalomyelitis by CD4+ T cells specific for an astrocyte protein, S100 beta. *Journal of neural transmission. Supplementum* 49: 43-51

Kornek B, Lassmann H. 1999. Axonal pathology in multiple sclerosis. A historical note. *Brain pathology* 9: 651-6

Lassmann H, Brunner C, Bradl M, Linington C. 1988. Experimental allergic encephalomyelitis: the balance between encephalitogenic T lymphocytes and demyelinating antibodies determines size and structure of demyelinated lesions. *Acta neuropathologica* 75: 566-76

Lennon VA, Kryzer TJ, Pittock SJ, Verkman AS, Hinson SR. 2005. IgG marker of optic-spinal multiple sclerosis binds to the aquaporin-4 water channel. *The Journal of experimental medicine* 202: 473-7

Lennon VA, Wingerchuk DM, Kryzer TJ, Pittock SJ, Lucchinetti CF, et al. 2004. A serum autoantibody marker of neuromyelitis optica: distinction from multiple sclerosis. *Lancet (London, England)* 364: 2106-12

Linington C, Berger T, Perry L, Weerth S, Hinze-Selch D, et al. 1993. T cells specific for the myelin oligodendrocyte glycoprotein mediate an unusual autoimmune inflammatory response in the central nervous system. *European journal of immunology* 23: 1364-72

Linington C, Bradl M, Lassmann H, Brunner C, Vass K. 1988. Augmentation of demyelination in rat acute allergic encephalomyelitis by circulating mouse monoclonal antibodies directed against a myelin/oligodendrocyte glycoprotein. *The American journal of pathology* 130: 443-54

Lucchinetti CF, Mandler RN, McGavern D, Bruck W, Gleich G, et al. 2002. A role for humoral mechanisms in the pathogenesis of Devic's neuromyelitis optica. *Brain : a journal of neurology* 125: 1450-61

Mader S, Lutterotti A, Di Pauli F, Kuenz B, Schanda K, et al. 2010. Patterns of antibody binding to aquaporin-4 isoforms in neuromyelitis optica. *PloS one* 5: e10455

Mandler RN, Davis LE, Jeffery DR, Kornfeld M. 1993. Devic's neuromyelitis optica: a clinicopathological study of 8 patients. *Annals of neurology* 34: 162-8

Misu T, Fujihara K, Kakita A, Konno H, Nakamura M, et al. 2007. Loss of aquaporin 4 in lesions of neuromyelitis optica: distinction from multiple sclerosis. *Brain : a journal of neurology* 130: 1224-34

Misu T, Fujihara K, Nakamura M, Murakami K, Endo M, et al. 2006. Loss of aquaporin-4 in active perivascular lesions in neuromyelitis optica: a case report. *The Tohoku journal of experimental medicine* 209: 269-75

Misu T, Fujihara K, Nakashima I, Sato S, Itoyama Y. 2005. Intractable hiccup and nausea with periaqueductal lesions in neuromyelitis optica. *Neurology* 65: 1479-82

Nakashima I, Fujihara K, Miyazawa I, Misu T, Narikawa K, et al. 2006. Clinical and MRI features of Japanese patients with multiple sclerosis positive for NMO-IgG. *Journal of neurology, neurosurgery, and psychiatry* 77: 1073-5

Neely JD, Christensen BM, Nielsen S, Agre P. 1999. Heterotetrameric composition of aquaporin-4 water channels. *Biochemistry* 38: 11156-63

Nicchia GP, Mastrototaro M, Rossi A, Pisani F, Tortorella C, et al. 2009. Aquaporin-4 orthogonal arrays of particles are the target for neuromyelitis optica autoantibodies. *Glia* 57: 1363-73

Nielsen S, Nagelhus EA, Amiry-Moghaddam M, Bourque C, Agre P, Ottersen OP. 1997. Specialized membrane domains for water transport in glial cells: high-resolution immunogold cytochemistry of aquaporin-4 in rat brain. *The Journal of neuroscience : the official journal of the Society for Neuroscience* 17: 171-80

Papadopoulos MC, Verkman AS. 2008. Potential utility of aquaporin modulators for therapy of brain disorders. *Progress in brain research* 170: 589-601

Paxinos G, Watson C. 1998. *The Rat Brain in Stereotaxic Coordinates*. San Diego, California: Academic Press.

Phuan PW, Ratelade J, Rossi A, Tradtrantip L, Verkman AS. 2012. Complement-dependent cytotoxicity in neuromyelitis optica requires aquaporin-4 protein assembly in orthogonal arrays. *The Journal of biological chemistry* 287: 13829-39

Pierson E, Simmons SB, Castelli L, Goverman JM. 2012. Mechanisms regulating regional localization of inflammation during CNS autoimmunity. *Immunological reviews* 248: 205-15

Pisani F, Mastrototaro M, Rossi A, Nicchia GP, Tortorella C, et al. 2011a. Identification of two major conformational aquaporin-4 epitopes for neuromyelitis optica autoantibody binding. *The Journal of biological chemistry* 286: 9216-24

Pisani F, Rossi A, Nicchia GP, Svelto M, Frigeri A. 2011b. Translational regulation mechanisms of aquaporin-4 supramolecular organization in astrocytes. *Glia* 59: 1923-32

Pittock SJ, Lennon VA, Krecke K, Wingerchuk DM, Lucchinetti CF, Weinshenker BG. 2006a. Brain abnormalities in neuromyelitis optica. *Archives of neurology* 63: 390-6

Pittock SJ, Weinshenker BG, Lucchinetti CF, Wingerchuk DM, Corboy JR, Lennon VA. 2006b. Neuromyelitis optica brain lesions localized at sites of high aquaporin 4 expression. *Archives of neurology* 63: 964-8

Pittock SJ, Weinshenker BG, Wijdicks EF. 2004. Mechanical ventilation and tracheostomy in multiple sclerosis. *Journal of neurology, neurosurgery, and psychiatry* 75: 1331-3

Pohl M, Fischer MT, Mader S, Schanda K, Kitic M, et al. 2011. Pathogenic T cell responses against aquaporin 4. *Acta neuropathologica* 122: 21-34

Pohl M, Kawakami N, Kitic M, Bauer J, Martins R, et al. 2013. T cell-activation in neuromyelitis optica lesions plays a role in their formation. *Acta neuropathologica communications* 1: 85

Popescu BF, Lennon VA, Parisi JE, Howe CL, Weigand SD, et al. 2011. Neuromyelitis optica unique area postrema lesions: nausea, vomiting, and pathogenic implications. *Neurology* 76: 1229-37

Poppe AY, Lapierre Y, Melancon D, Lowden D, Wardell L, et al. 2005. Neuromyelitis optica with hypothalamic involvement. *Multiple sclerosis* 11: 617-21

Rash JE, Yasumura T, Hudson CS, Agre P, Nielsen S. 1998. Direct immunogold labeling of aquaporin-4 in square arrays of astrocyte and ependymocyte plasma membranes in rat brain and spinal cord. *Proceedings of the National Academy of Sciences of the United States of America* 95: 11981-6

Roemer SF, Parisi JE, Lennon VA, Benarroch EE, Lassmann H, et al. 2007. Pattern-specific loss of aquaporin-4 immunoreactivity distinguishes neuromyelitis optica from multiple sclerosis. *Brain : a journal of neurology* 130: 1194-205

Rossi A, Crane JM, Verkman AS. 2011. Aquaporin-4 Mz isoform: brain expression, supramolecular assembly and neuromyelitis optica antibody binding. *Glia* 59: 1056-63

Rossi A, Pisani F, Nicchia GP, Svelto M, Frigeri A. 2010. Evidences for a leaky scanning mechanism for the synthesis of the shorter M23 protein isoform of aquaporin-4: implication in orthogonal array formation and neuromyelitis optica antibody interaction. *The Journal of biological chemistry* 285: 4562-9

Sinclair C, Kirk J, Herron B, Fitzgerald U, McQuaid S. 2007. Absence of aquaporin-4 expression in lesions of neuromyelitis optica but increased expression in multiple sclerosis lesions and normal-appearing white matter. *Acta neuropathologica* 113: 187-94

Storch MK, Stefferl A, Brehm U, Weissert R, Wallstrom E, et al. 1998. Autoimmunity to myelin oligodendrocyte glycoprotein in rats mimics the spectrum of multiple sclerosis pathology. *Brain pathology* 8: 681-94

Takahashi T, Fujihara K, Nakashima I, Misu T, Miyazawa I, et al. 2006. Establishment of a new sensitive assay for anti-human aquaporin-4 antibody in neuromyelitis optica. *The Tohoku journal of experimental medicine* 210: 307-13

Takahashi T, Fujihara K, Nakashima I, Misu T, Miyazawa I, et al. 2007. Anti-aquaporin-4 antibody is involved in the pathogenesis of NMO: a study on antibody titre. *Brain : a journal of neurology* 130: 1235-43

Vass K, Heininger K, Schafer B, Linington C, Lassmann H. 1992. Interferon-gamma potentiates antibody-mediated demyelination in vivo. *Annals of neurology* 32: 198-206

Verbavatz JM, Ma T, Gobin R, Verkman AS. 1997. Absence of orthogonal arrays in kidney, brain and muscle from transgenic knockout mice lacking water channel aquaporin-4. *Journal of cell science* 110 (Pt 22): 2855-60

Verkman AS, Anderson MO, Papadopoulos MC. 2014. Aquaporins: important but elusive drug targets. *Nature reviews. Drug discovery* 13: 259-77

Waters P, Vincent A. 2008. Detection of anti-aquaporin-4 antibodies in neuromyelitis optica: current status of the assays. *International MS journal / MS Forum* 15: 99-105

Weinshenker BG. 2003. Neuromyelitis optica: what it is and what it might be. *Lancet (London, England)* 361: 889-90

Wingerchuk DM, Hogancamp WF, O'Brien PC, Weinshenker BG. 1999. The clinical course of neuromyelitis optica (Devic's syndrome). *Neurology* 53: 1107-14

Wingerchuk DM, Lennon VA, Lucchinetti CF, Pittock SJ, Weinshenker BG. 2007. The spectrum of neuromyelitis optica. *The Lancet. Neurology* 6: 805-15

Wingerchuk DM, Lennon VA, Pittock SJ, Lucchinetti CF, Weinshenker BG. 2006. Revised diagnostic criteria for neuromyelitis optica. *Neurology* 66: 1485-9

Wingerchuk DM, Weinshenker BG. 2003. Neuromyelitis optica: clinical predictors of a relapsing course and survival. *Neurology* 60: 848-53

Yamamoto K, Matsunaga S, Matsui M, Takeda N, Yamatodani A. 2002. Pica in mice as a new model for the study of emesis. *Methods and findings in experimental and clinical pharmacology* 24: 135-8

Yang B, Brown D, Verkman AS. 1996. The mercurial insensitive water channel (AQP-4) forms orthogonal arrays in stably transfected Chinese hamster ovary cells. *The Journal of biological chemistry* 271: 4577-80

Zeka B, Hastermann M, Hochmeister S, Kogl N, Kaufmann N, et al. 2015. Highly encephalitogenic aquaporin 4-specific T cells and NMO-IgG jointly orchestrate lesion location and tissue damage in the CNS. *Acta neuropathologica* 130: 783-98